

Slow-moving rock glaciers in marginal periglacial environment of Southern Carpathians

Alexandru Onaca^{1,2}, Flavius Sîrbu², Valentin Poncoş³, Christin Hilbich⁴, Tazio Strozzi⁵, Petru Urdea^{1,2}, Răzvan Popescu⁶, Oana Berzescu², Bernd Etzelmüller⁷, Alfred Vespremeanu-Stroe⁶, Mirela Vasile⁸, Delia Teleagă³, Dan Birtaş³, Iosif Lopătiță¹, Simon Filhol⁷, Alexandru Hegyi^{2,7}, Florina Ardelean¹

¹Department of Geography, West University of Timișoara, Timișoara, Romania

²Institute for Advanced Environmental Research, West University of Timișoara, Timișoara, Romania

³Terrasigna, Bucharest, Romania

⁴Department of Geosciences, University of Fribourg, Fribourg, Switzerland

⁵Gamma Remote Sensing, Gümligen, Switzerland

⁶Faculty of Geography, University of Bucharest, Bucharest, Romania

⁷Department of Geosciences, University of Oslo, Oslo, Norway

⁸Division of Earth, Environmental and Life Sciences, University of Bucharest Research Institute, Bucharest, Romania

Correspondence to: Flavius Sîrbu (flavius.sirbu@e-uvr.ro)

Abstract. Rock glaciers, composed of debris and ice, are widely distributed across cold mountain regions worldwide. Although research on rock glaciers is gaining momentum, the distinct behaviour of rock glaciers in the marginal periglacial environments remains poorly understood. In this study, we combine remote sensing and in situ methods to gain insights into the characteristics of transitional rock glaciers in the Carpathian Mountains. We applied Persistent Scatterer Interferometry (PSInSAR) to Sentinel-1 images from 2015 to 2020 to identify areas with slope movements associated with rock glaciers and differential GNSS measurements (2019-2021) to detect the horizontal movement of 25 survey markers. Continuous ground temperature monitoring and measurements of the bottom temperature of the winter snow cover were used to examine the energy exchange fluxes characteristics of transitional rock glaciers in the Carpathians. The subsurface of one transitional rock glacier was investigated using geophysical measurements (electrical resistivity tomography and refraction seismic tomography), while petrophysical joint inversion was used to quantify the ice content. The PSInSAR methodology identified 92 moving areas (MAs) with low displacement rates ($< 5 \text{ cm yr}^{-1}$). These MAs were generally located between 2000 and 2300 meters where solar radiation was minimal. Near-surface thermal measurements on four rock glaciers indicate favorable conditions for permafrost persistence, largely driven by internal ventilation processes (e.g., advection heat fluxes) throughout the winter. Very low ground surface temperatures were detected by BTS measurements over much of the investigated rock glaciers, particularly in their upper parts and within the MAs. Geophysical investigations reveal remnants of ice-poor permafrost within the Galeșu rock glacier, while petrophysical joint inversion modelling indicates a low ground ice content ($\sim 18 \%$) in its upper sector. At this site, the recorded surface displacements are more likely the result of ice-melt-induced

33 subsidence, solifluction, or the tilting and sliding of blocks within the active layer. The flow direction of dGNSS markers at
34 two rock glaciers indicated consistent movement toward their fronts, a pattern typical of permafrost creep. Regarding activity
35 status, the majority of rock glaciers in the Retezat Mountains were categorized as relict, with only 21% classified as transitional.
36 Compared to relict rock glaciers, transitional ones are situated at a median elevation 150 m higher and have a slightly smaller
37 median size.

38 **1 Introduction**

39 Rock glaciers are prominent landforms in the periglacial environment, serving as indicators of permafrost presence at the time
40 of their formation (Haeberli et al., 2006). Generated through past or present permafrost creep, they are debris-dominated
41 features typically identified by their front, lateral margins and occasionally ridge-and-furrow surface patterns (RGIK, 2023a).
42 The geomorphic imprint of permafrost creep is often preserved even after the ice within the rock glacier has completely melted
43 (Kellerer-Pirklbauer et al., 2022). In the Southern Carpathians, rock glaciers mostly present as relict landforms, yet retain
44 isolated permafrost in certain areas (Vespremeanu-Stroe et al., 2012; Onaca et al., 2013, 2015; Popescu et al., 2015, 2024).
45 Indicators such as extensive lichen cover, vegetated fronts and the overall morphological stability of many landforms suggest
46 that permafrost creep is significantly reduced compared to the colder climatic conditions of the pre-Holocene (Popescu et al.,
47 2017). These rock glaciers are predominantly mantled by angular, coarse-grained blocks which facilitate ground cooling
48 (Onaca et al., 2017a). The thermal offset associated with this blocky surface layer contributes to the maintenance of subzero
49 temperatures in the subsurface over prolonged periods (Kellerer-Pirklbauer, 2019), thereby enhancing permafrost preservation
50 even at relatively low altitudes (Colucci et al., 2019). In addition, the `chimney effect` - an advective heat flux process
51 (Delaloye and Lambiel, 2005) - significantly contributes to surface cooling in highly porous, openwork structures.
52 Permafrost creep encompasses both the internal deformation of ice within the frozen material and shearing at discrete planes
53 within or just beneath the frozen structure (Cicoira et al., 2021). Surface displacement can also result from processes occurring
54 within the active layer, such as ice-melt-induced subsidence, solifluction, or the tilting and sliding of blocks, which may act
55 independently of or in addition to permafrost creep (Serrano et al., 2010; Cicoira et al., 2021). The surface kinematics of rock
56 glaciers had garnered significant interest from the international community in recent years (Kellerer-Pirklbauer et al., 2024;
57 Kääb and Røste, 2024; Pellet et al., 2024; Hu et al., 2025) due to the growing need to better understand how mountain
58 permafrost responds to ongoing climate change. While the response of rock glaciers to present-day air temperature rising is
59 intricate in many instances, increased rock glacier velocities has been linked to warmer climate (Wirz et al., 2016; Cicoira et
60 al., 2019; Kenner et al., 2019; Kääb et al., 2021; Marcer et al., 2021; Kellerer-Pirklbauer et al., 2024). Rising temperatures
61 within frozen debris enhance movement rates, as warming reduces the viscosity of the ice and promotes additional lubrication
62 from infiltrating water (Kääb et al., 2007). According to Necsoiu et al. (2016), slow-moving rock glaciers in the Southern
63 Carpathians exhibited increased velocities between 2007 and 2014, attributed to rising permafrost temperatures. Annual rates
64 of horizontal surface kinematics of rock glaciers range from a few millimetres to a few meters (Strozzi et al., 2020), though

destabilization can result in velocities exceeding ten meters per year (Roer et al., 2008; Delaloye et al., 2013; Eriksen et al., 2018; Marcer et al., 2021; Hartl et al., 2023).

Many studies have demonstrated the feasibility of satellite radar interferometry (InSAR) for kinematic analysis of rock glaciers, capable of detecting motion at the millimetre scale (Liu et al., 2013; Necsoiu et al., 2016; Strozzi et al., 2020; Bertone et al., 2022). This technique enables the mapping of land surface deformation with an appropriate spatial and temporal resolution over vast areas (Bertone et al., 2022). Surface displacements can be attributed to permafrost creep only if the flow direction and velocity remain spatially consistent and uniform over a documented period (RGIK, 2023a). Permafrost creep typically occurs when the thickness of the ice-rich core in rock glaciers reaches at least 10-25 m (Cicoira et al., 2021). In contrast, displacements observed in rock glaciers with thinner layers of frozen debris are primarily driven by deformations within the active layer above the permafrost table.

While rock glaciers in discontinuous permafrost have been extensively studied, the distinctive behaviour of those in marginal periglacial environments has received far less attention (Serrano et al., 2010; Necsoiu et al., 2016). In such settings, rock glaciers exhibit either no movement or significantly slower movement rates (a few cm yr^{-1}) and are often referred to as transitional rock glaciers (RGIK, 2023a). This reduced surface velocity is attributed to the high shear strength of the material, which inhibits fast creep movement (Cicoira et al., 2021). Even if slow-moving rock glaciers were documented in various regions of the world (Brencher et al., 2021; Bertone et al., 2022; Lilleøren et al., 2022; Lambiel et al., 2023), the relationship between their velocity and ground ice content was rarely addressed (Serrano et al., 2010). Since borehole information is limited in high and remote mountains, a promising alternative to quantitatively estimate ground ice content is using petrophysical joint inversion (PJI) of seismic refraction and electrical resistivity data (Wagner et al., 2019).

The Southern Carpathian range is a key region in Europe where transitional rock glaciers are studied. Here, the enhanced continentality effects induce a distinct pattern of manifestation of periglacial phenomena compared with other mid-latitude mountains in Europe (Onaca et al., 2017a). In marginal periglacial mountains, permafrost occurrence is generally sporadic or patchy and site-specific characteristics highly control its distribution (Stiegler et al., 2014; Onaca et al., 2015; Kellerer-Pirklbauer, 2019; Popescu et al., 2024). Above 2000 m in the Southern Carpathians, the 1991-2020 climatological period was 0.8 °C warmer than the 1961-1990 baseline (Berzescu et al., 2025).

The paper aims to present new results on the rock glaciers dynamics and permafrost characteristics in the Retezat Mountains and, more broadly, to better understand the behaviour of rock glaciers in marginal periglacial mountains. To achieve this goal, we will (i) locate and assess the kinematics of rock glaciers' moving areas using SAR-based persistent scatterers interferometry (PSInSAR); (ii) update the existing rock glacier inventory in the Retezat Mountains with information on the rock glacier dynamics; (iii) estimate ground ice content using petrophysical joint inversion based on electrical resistivity and seismic refraction data and (iv) characterise the thermal conditions at the rock glaciers surface.

96 2. Study area

97 The Retezat Mountains are among the highest massifs in the Romanian Carpathians, constituting a distinct part of the Southern
98 Carpathians (the latter are also known as the Transylvanian Alps). Located in the western part of the Southern Carpathians
99 (45°22' N and 22°53' E), the Retezat Mountains reach an elevation of 2500 m, revealing a typical alpine landscape (Fig. 1).

100 The climate in this region can be characterised as a moderate temperate continental climate, classified within the subarctic or
101 boreal category according to the Köppen classification system. Between 2000 and 2100 m elevation, the mean annual air
102 temperature is approximately 0° C, annual precipitation averaging around 1000 mm (calculated for the period 1961-2007)
103 (Onaca et al., 2017a).

104 The mountain range is part of the orogenic units spanning two distinctive tectonic-structural regions: the Danubian Domain
105 and the Getic Domain, both with the status of a thrust sheet. The Danubian Domain, referred to as the Danubian Autochthonous,
106 is primarily characterised by two dominant granitic bodies, Retezat and Buta (Pavelescu, 1953). These granitic bodies are
107 surrounded in the marginal area by epi- and meso-metamorphic schists, typifying the Getic Nappe. Specific Mesozoic rocks,
108 particularly limestones, are prevalent in the southern part of this mountain range (Urdea, 2000). 87 % of the rock glaciers in
109 the Retezat Mountains have developed on granite bedrock (Fig. 2), while the remaining landforms are situated on metamorphic
110 schists.

111 The Retezat Mountains boast one of the most comprehensive and distinct arrays of glacial and periglacial landforms in the
112 Romanian Carpathians. Notably, they host the largest glacial cirques in the Romanian Carpathians, with a combined area of

all glacial cirques amounting to c. 8 % of the massif's total area (Urdea, 2000). During the Last Glacial Maximum (LGM) (20.6 ka), glaciers in these mountains reached lower elevations ranging from 1000 to 1300 m (Ruszkiczay-Rüdiger et al., 2021).

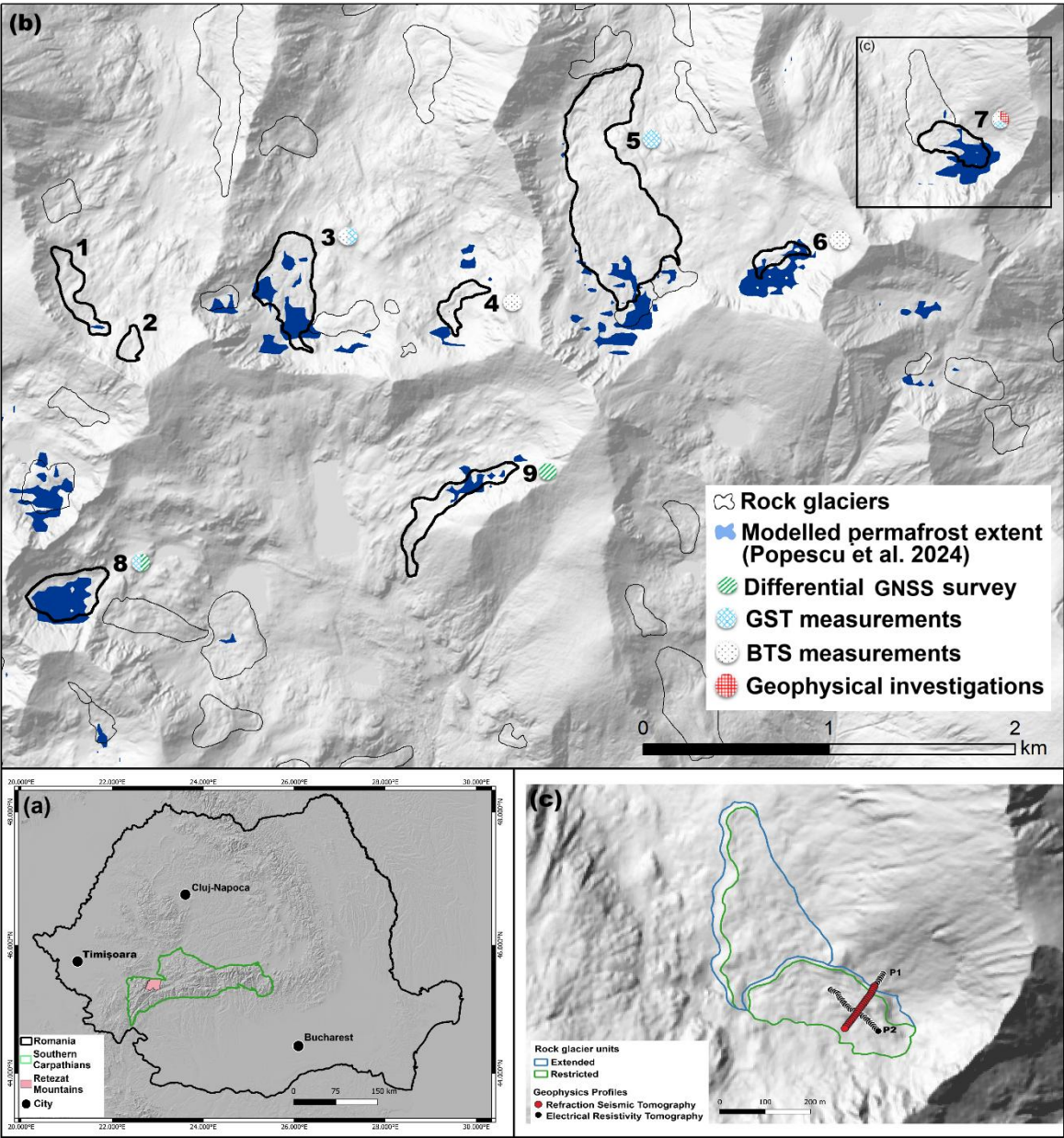
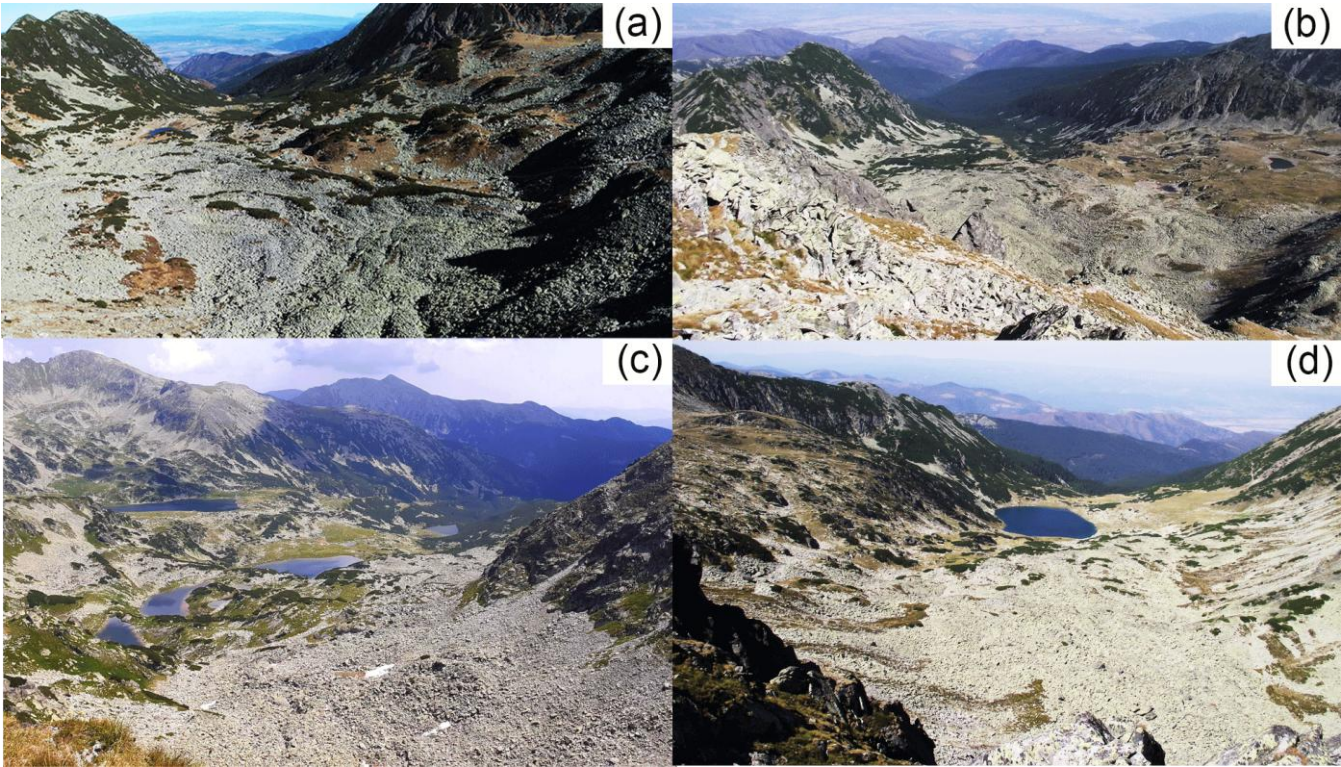


Figure 1: Study sites. (a) Overview map with the location of the Retezat Mountains in the Southern Carpathians and in Romania, background of the map: hillshade based on FABDEM (Howker et al. 2022). (b) modelled permafrost extent (Popescu et al., 2024) and spatial distribution of rock glaciers in the Retezat Mountains overlaid on a hillshade based on the LAKI II DEM (LAKI II MNT, 2024). The rock glaciers that are discussed in the present paper are numbered (1 - Stânişoara, 2 - Bucura, 3 - Pietrele, 4 - Pietricelele, 5 - Valea Rea, 6 - Păpuşa, 7 - Galeşu, 8 - Judele, 9 - Berbecilor), and the ground based measurements that have been performed on each of them are represented by a composite symbol near the number. (c) A detailed map with the position of the geophysics profiles on Galeşu rock glacier; note: same background image as (b).

123 Subsequently, the Late Glacial period witnessed five phases of deglaciation. However, no glacial advance has been
124 documented in the central part of the Retezat Mountains during or after the Younger Dryas based on cosmic-ray exposure
125 dating (Ruszkiczay-Rüdiger et al., 2021). Rock glaciers in the Retezat Mountains likely began to develop during the Younger
126 Dryas, with most having become relict or transitional since the onset of the Holocene. Permafrost associated with rock glaciers
127 had been documented since 1993 in this mountain range (Urdea, 1993). A recent inventory described Retezat Mountains as
128 the range with the highest number (94) and density (0.52 landforms/km², and 2.87 ha/km² at altitudes above 1540 meters) of
129 rock glaciers in the Romanian Carpathians (Onaca et al., 2017b) (Fig. 1). Additionally, they harbour the longest Carpathian
130 rock glacier, Valea Rea, extending 1.4 km (Urdea, 2000) (Fig. 2b).



131
132 **Figure 2: Pictures of the rock glaciers in the Retezat Mountains: (a) Pietrele; (b) Valea Rea; (c) Judele; (d) Galeșu. Photo credit: A.**
133 **Onaca.**

134 **3. Methods**

135 **3.1. Rock glacier inventory**

136 Rock glaciers are categorised into three types based on their activity status: active, transitional, or relict, as outlined by (RGIK,
137 2023a). Active rock glaciers exhibit consistent downslope movement across most of their surface with displacement rates
138 ranging from a decimetre to several meters per year (RGIK, 2023a). Most of the surface of a transitional rock glacier
139 experiences little to no downslope movement, with annual average displacement rates generally falling below one decimetre

140 (RGIK, 2023a). Rock glaciers exhibiting no detectable movement across most of their surface are classified as relict (RGIK,
141 2023a).

142 This study revised the existing inventory of rock glaciers in the Southern Carpathians (Onaca et al., 2017b) in accordance with
143 the guidelines provided by RGIK (2023a). The inventory involved mapping rock glaciers through fieldwork surveys and
144 detailed examination of high-resolution aerial imagery. Due to the availability of kinematic information for only a limited
145 number of landforms (Vespremeanu-Stroe et al., 2012; Necsoiu et al., 2016), the current inventory lacks data on the activity
146 of rock glaciers. Information on rock glacier kinematics was only available for a few landforms (Vespremeanu-Stroe et al.,
147 2012; Necsoiu et al., 2016), while most of the rock glaciers were classified as either intact or relict based on geomorphological
148 and ecological criteria (e.g., degree and type of vegetation cover).

149 **3.2. Persistent scatterer interferometry using Sentinel-1 data**

150 PSInSAR is a remote sensing technique designed to measure ground displacements along the radar line of sight (SAR LOS)
151 with millimetric accuracies (Rucci et al., 2012; Yu et al., 2020). Although Sentinel-1 (S1) SAR data does not offer the highest
152 possible spatial resolution, its worldwide periodic coverage and open data policy has enabled wide-scale monitoring since
153 2014, leading to a thriving archive of ground-motion products with various applications.

154 Sentinel-1 serves as the backbone of the operational PSInSAR application development for the European Ground Motion
155 Service (EGMS), openly available throughout the entire European area. The PSInSAR analysis employed in this study was
156 developed by Terrasigna and generally follows the EGMS specifications ([https://land.copernicus.eu/en/technical-library/egms-
157 algorithm-theoretical-basis-document/@@download/file](https://land.copernicus.eu/en/technical-library/egms-algorithm-theoretical-basis-document/@@download/file)). However, there are a few differences, particularly related to the
158 choice of reference points, the modelling of atmospheric effects in steep terrain and the selection of SAR images. EGMS
159 products are computed at the regional level, where reference points are typically located in lowland areas covered by
160 infrastructure, which provides strong and stable radar backscattering. Additionally, EGMS includes all available acquisitions,
161 even those affected by snow cover at high altitudes. However, inspection of EGMS products reveals that extending the
162 measurement network from lowland reference points to mountain summits was largely unsuccessful. This is mainly because
163 the atmospheric path delay associated with steep topography was not adequately compensated for and acts like phase noise.
164 Furthermore, snow cover during winter significantly impacts data quality. Non-homogeneous snow or snow with variable
165 humidity scatters radar signals and increases phase noise. In the case of dry snow, radar waves penetrate the snowpack, but
166 because they propagate more slowly than in air, the interferometric phase experiences a time delay. This delay produces
167 apparent subsidence (false ground displacement away from the radar sensor). Combined these factors often result in the
168 rejection of radar targets on mountain tops due to excessive noise.

169 To address these issues, Terrasigna carefully selected reference points located on mountain summits, where the topographic
170 atmospheric delay is similar to that of the areas of interest. Additional efforts were made to improve the accuracy of
171 atmospheric delay modelling and compensation. Furthermore, only snow-free acquisitions were considered. As a result, the
172 high density of radar targets – formed by bare rocks at the top of the mountains – is preserved in our measurements.

Both ascending and descending paths were processed for cross-validation, along with L-band ALOS data, which was analyzed for the same purpose. Because descending passes occur in the early morning – when atmospheric conditions are generally more stable than in the evening – the resulting measurements tend to be less noisy. A 2D decomposition between ascending and descending passes is technically feasible; however, the steep topography introduces several challenges. First, areas that are clearly visible from one orbit may be in shadow or appear foreshortened in the other, reducing data quality and spatial consistency. Second, since the topography is steep, the preferential direction of ground movement is often dictated by the slope of the terrain. Additionally, the 2D decomposition estimates vertical and east-west displacement components under the assumption that there is no north-south movement – an assumption that is frequently invalid in mountainous regions, where north-south displacement is commonly observed. Based on these issues, it was decided to use the orbits that yielded the best results for validation and mapping.

Figure 3a illustrates the total coverage (from all available S1 paths from both the Ascending and Descending orbits) of the EGMS product in the area of interest, while Figure 3b illustrates the PSInSAR analysis of the same area, derived solely from one S1 path (Path 80 Descending). In the following, this is referred to as ‘Terrasigna PSInSAR’. It is evident that the EGMS coverage is relatively sparse and does not highlight dynamic areas – there are no zones marked in red, which typically indicate significant ground motion. In contrast, the PSInSAR results from Terrasigna show much denser coverage and clearly identify dynamic areas, with red colors representing higher displacement rates. In general, there are technical differences in the computation of data across EGMS products, primarily due to the involvement of multiple groups in the project. Terrasigna’s algorithms are more closely aligned with those used for the EGMS in southern Europe, which appear to offer better extraction of non-linear motion.

In this study, the kinematics of the rock glaciers were assessed using 181 images acquired between May 15, 2015, and October 4, 2021, covering only the snow-free periods to avoid coherence loss. The motion was measured along the SAR LOS direction; however, the actual displacement of the rock glacier surface is expected to mainly occur along the slope or in the vertical direction. The PSInSAR algorithm, as described by Rucci et al. (2012), Crosetto et al. (2016) and Ponçoş et al. (2022), preserved all displacement information to maximize the chances of detecting slow movements (mm yr^{-1}) in areas without vegetation cover. The process began by extracting linear deformation information before applying any spatial or temporal filtering, which was typically used to improve phase statistics. A key challenge is that the atmospheric phase is two orders of magnitude larger than the displacement signal (Ponçoş et al., 2022), requiring meticulous phase unwrapping and correction of each residual interferogram. Due to significant atmospheric noise in steep terrain or in areas with large elevation differences, a reference point at a similar elevation to the rock glaciers was chosen on the mountain summit. This approach minimizes atmospheric phase differences, improving coherence and reliability of the PSInSAR measurements. An important number of rock glaciers in the area are oriented north-south or south-north, which may lead to an underestimation of actual displacements due to the limited sensitivity of the satellite look angle to slope-parallel motion.

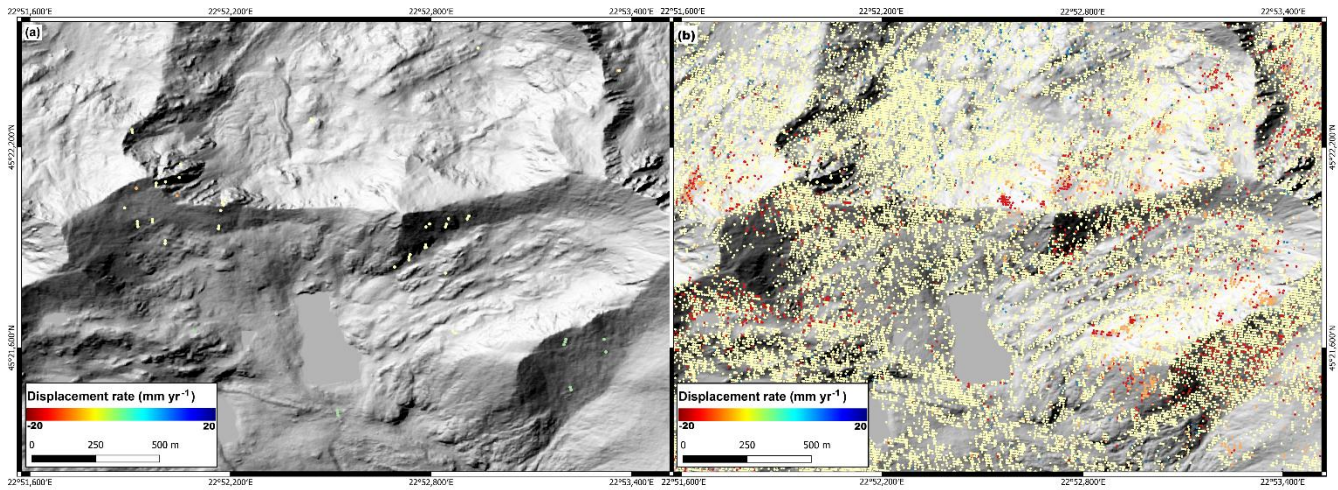


Figure 3: Comparison between the PSInSAR spatial density of measurements obtained by EGMS (a) and Terrasigna (b) in the central area of Retezat Mountains. Background of both maps: hillshade based on the LAKI II DEM (LAKI II MNT, 2024).

The PSInSAR results were analysed using the Persistent Scatterers Online Software Tool (PSTool), a web-based platform developed by Terrasigna Inc. (Poncoş et al., 2022), to exploit a large volume of ground displacement data. The PSTool platform can be used to inspect temporal characteristics of the ground motion, select areas of interest and extract temporal averages of displacement rates, export temporal profiles to standard formats for integration in the user's own platforms and upload user-specific layers on top of the displacement information.

3.3. Inventorying moving areas

According to RGIK (2023a) guidelines, a moving area (MA) represents an area at the surface of the rock glacier characterised by relatively homogeneous velocity rates and consistent flow direction. Based on multi-annual surface velocity rates, MAs were identified and delineated within the inventoried rock glaciers (Onaca et al., 2017b) using Terrasigna PSInSAR results. The next step was to assign velocity classes to moving areas considering the standardised velocity classes (Barboux et al., 2014; Bertone et al., 2022). In our case, MAs were attributed to one of the following SAR LOS deformation velocity classes: undefined, 0.3-1 cm yr⁻¹, 1-3 cm yr⁻¹, and 3-10 cm yr⁻¹ (RGIK, 2023a) (Fig. 4). The velocity class characterizes the average yearly displacement rate recorded within a MA during the 2015–2021 period. The undefined category was assigned to MAs characterised by inhomogeneous velocity rates. PSInSAR-based surface displacement of ≤ 0.3 cm yr⁻¹ were assigned to the “no movement” category, as this threshold was considered the lower limit of velocity detection on S1 interferograms in this type of approach (Rouyet et al., 2021). The moving areas were manually digitized and compiled into an inventory using ArcGIS 10.8. Since many surface displacements in marginal periglacial regions result from active layer deformations (e.g., melt-induce subsidence), we have set the minimum area for an MA at 1000 m² to exclude those not associated with permafrost creep. For

227 the spatial analysis of the rock glaciers and MAs, we used a one-meter resolution digital elevation model generated from high-
228 resolution LiDAR source data acquired in 2018 (LAKI II MNT, 2024).

229 **3.4. Differential GNSS measurements**

230 Judele (8) and Berbecilor (9) rock glaciers had been surveyed by differential GNSS (DGNSS) measurements every summer
231 between 2019 and 2021. A differential dual-frequency Topcon Hiper V GPS had acquired high-precision positioning data in
232 real-time kinematics mode. The dGNSS device uses two receivers, one installed as a fixed base station, whereas the roving
233 receiver was moved to different points of interest in the field. The mobile receiver gets the corrected position information
234 calculated by the base station via a radio signal in order to measure a point with very high precision (i.e. < 1 cm accuracy in
235 the horizontal plane). 25 survey markers were measured in October 2019 and remeasured in October 2020 and 2021. Two
236 points outside the boundaries of the rock glaciers, located on stable bedrock, were also measured to assess the horizontal
237 accuracy of the DGNSS. The difference between the yearly measurements in both cases indicated an accuracy range of 0.3 to
238 0.6 mm/yr⁻¹. The mean DGNSS velocities used in the analysis were calculated as the yearly displacement between the initial
239 and final position over a two-year period.

240 **3.5. Validation with ALOS-2 PALSAR-2 interferometry**

241 To further validate Terrasigna's PSInSAR analysis specifically developed for this study, we considered a series of six ALOS-
242 2 PALSAR-2 images regularly acquired between 2014 and 2019 at the end of the snow-free season in September and October.
243 We computed wrapped differential interferograms with time intervals ranging from one to five years using a DEM with 10 m
244 pixel spacing obtained from 1:25 000 scale topographic maps with a contour interval of 10 m. For the interpretation of the
245 interferograms, we followed the practical guidelines of the IPA Action Group Rock glacier inventories and kinematics (RGIK,
246 2023b).

247 **3.6. Thermal conditions**

248 The bottom temperature of the winter snow cover (BTS) is an efficient method to map permafrost distribution in non-arid
249 mountains (Vonder Mühl et al., 2002). If optimum snow conditions are met, the BTS values indicate probable permafrost at
250 < -3 °C, possible permafrost at -2 to -3 °C and absence of permafrost at > -2 °C (Haeberli, 1973; Hoelzle, 1992; Popescu et al.,
251 2024). However, in dry, porous bouldery surfaces where air convection and advection occur, this method lacks the precision
252 needed to accurately map permafrost occurrence (Bernhard et al., 1998). Nevertheless, the BTS method remains highly
253 effective for distinguishing areas with colder ground surface temperatures from those with warmer ones. Two classical 2.6 m
254 long BTS probes equipped with digital thermometers (0.5 °C precision) were used to measure 140 thermal records at the snow-
255 ground interface. The BTS measurements were acquired at the end of March 2022 on four rock glaciers in three north-facing
256 valleys in the central part of the Retezat Mountains (Fig. 1). At all the sites where BTS values were recorded, the snow was
257 sufficiently thick (> 80 cm) to insulate the ground from external air temperature fluctuations (Ishikawa et al., 2003). Previous

studies in the Southern Carpathians (Vespremeanu-Stroe et al., 2012; Onaca et al., 2015) revealed that in March, BTS values remain nearly constant below a thick snow cover, which usually falls in November or December. Minimal temperature data loggers became widely used in mountain permafrost terrain to get more detailed insights into the energy exchange fluxes at the surface of rock glaciers (Hoelzle et al., 1999). Four rock glaciers in the central part of the Retezat Mountains were selected to monitor the thermal regime at the ground surface (Fig. 1b). The evolution of ground surface temperature (GST) was recorded using iButtons DS1922L data loggers. According to the producer, the miniature thermistors used in this study have an accuracy of ± 0.5 °C and measure temperatures between -40 and 80°C. The sensors were indirectly calibrated at 0 °C using the snow melting period (“zero curtain” interval), and GST data were measured and logged every 2 hours. In mid and late winter, the ground surface temperature remains stable under a thick insulating layer, and the subsurface mainly controls the energy flux. This is why the “winter equilibrium temperature” (WEqT) is considered an excellent empirical predictor of permafrost existence if temperatures are low (i.e., < -2 °C) (Sattler et al., 2016). WEqT refers to stable ground surface temperature period lasting at least two weeks, generally occurring in late winter, when snow cover exceeds 50 cm in thickness (Schoeneich, 2011). WEqT and mean annual ground surface temperature (MAGST) were calculated for each GST monitoring site.

3.7. Geophysical Methods and PJI Modelling

Geophysical methods, such as electrical resistivity tomography (ERT) and refraction seismic tomography (RST), are widely applied in mountain permafrost studies and have the potential to characterise subsurface structure and heterogeneity and detect and map ground ice occurrences (Hauck et al., 2011; Herring et al., 2023). Both methods are sensitive to differences between frozen and unfrozen subsurface conditions. As ice can be considered an electrical insulator as opposed to water, the electrical resistivity increases exponentially with decreasing temperatures below 0 °C. Similarly, the seismic P-wave velocity of ice is with 3500 m s^{-1} significantly higher than that of liquid water ($\sim 1500 \text{ m s}^{-1}$) or air (330 m s^{-1}), allowing to differentiate between frozen sediments (containing ice) and unfrozen sediments (pore space filled with water or air).

ERT is the most common geophysical technique applied in permafrost research and is used for mapping permafrost occurrence where no borehole information is available, as well as monitoring changes in the ice-to-water ratio (Wagner et al., 2019; Mollaret et al., 2020). The RST method is often used as a complementary method to ERT to reduce the ambiguity in the interpretation of ERT data, as the P-wave velocity v_p is mainly controlled by density, and variations in v_p allow to identify porosity changes, or discriminate between liquid (water) and solid (ice) pore fluid, as well as in determining the depth to the bedrock.

In the absence of ground truth information about the state of permafrost, another advantage of geophysical data is, that co-located ERT and RST data can be used to quantitatively estimate the content of the four phases (i.e., rock, ice, water and air) using the so-called 4-phase model approach, which is based on the petrophysical equations by Archie (1942) for the electrical resistivity and that of Timur (1968) for the P-wave velocity.

290 Recently, the approach has been further developed by Wagner et al. (2019), to the so-called petrophysical joint inversion (PJI)
291 framework, permitting the joint inversion of ERT and RST data sets to simultaneously solve for the subsurface distribution of
292 the 4 phases. The main advantage of the PJI is the increased accuracy of the parameters estimated, as the algorithms iteratively
293 search for a subsurface model that simultaneously explains the seismic and resistivity measurements. This is especially relevant
294 for the porosity model, which is represented more realistically in the PJI than in previous versions of the 4-phase model (Hauck
295 et al., 2011). Mollaret et al. (2020) demonstrated the applicability of the PJI for data collected on different alpine permafrost
296 landforms with different ice contents.

297 In the field, 2D ERT data were collected using a GEOTOM (Geolog) multi-electrode instrument equipped with 50 electrodes
298 spaced 4 meters apart. By combining a multitude of individual measurements with different electrode combinations (i.e.
299 quadrupoles) along a profile line, a 2-dimensional resistivity model of the subsurface is obtained. All measurements were
300 performed in the Wenner configuration to ensure an optimal signal-to-noise ratio, which is especially important in dry and
301 coarse-blocky terrain.

302 2-dimensional RST data were obtained using a 24-channel Geode seismometer (Geometrics). An artificial seismic wave is
303 produced by hitting a sledgehammer to the ground, and the waves travel along different paths through the subsurface and back
304 to the surface, where they are registered by 24 geophones. The subsurface structure and composition can be derived from the
305 travel time the so-called P-wave needs from the source (i.e. hammer) to the geophones. The wave velocity (v_p in m s^{-1}), and
306 thus the travel time, is basically a function of the density of the subsurface material, and the obtained seismic velocity allows
307 inferring the subsurface material. The pre-processing of the seismic field data (picking of first arrivals) was performed using
308 the software *ReflexW* (Sandmeier, 2020). The individual ERT and RST data sets were first independently inverted using the
309 PyGimLi framework (Rücker et al., 2017), and in a second step, the PJI was conducted to estimate ground ice contents using
310 the approach developed by (Wagner et al., 2019).

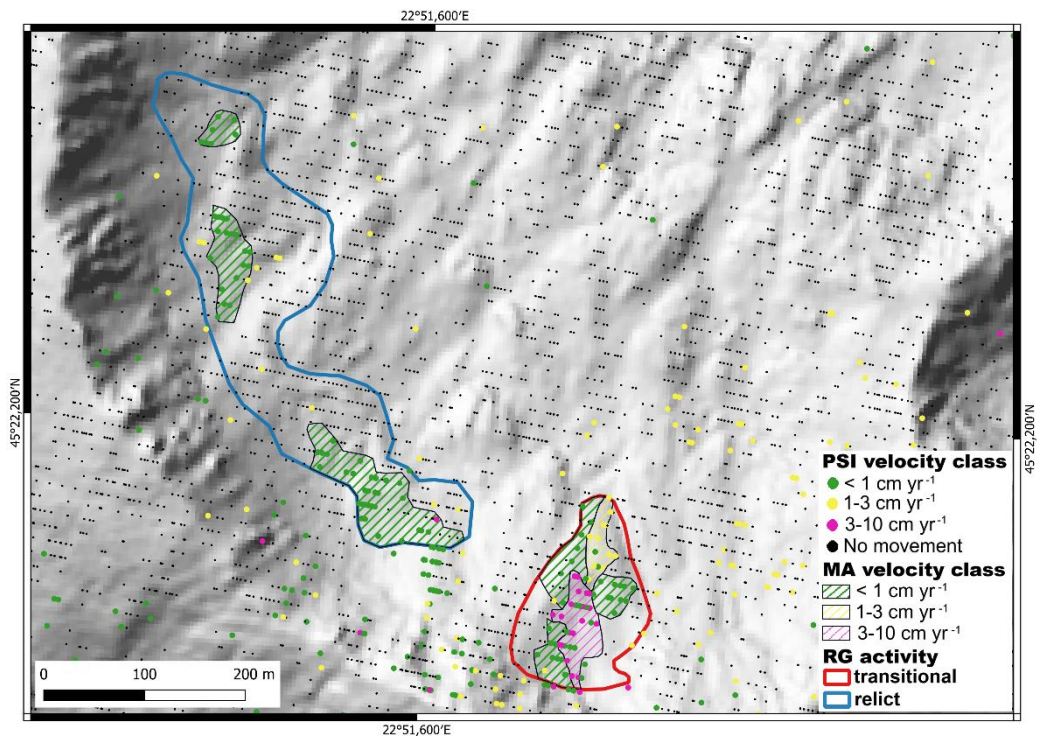
311 4. Results

312 4.1. Inventorying moving areas

313 In the Retezat Mountains the MAs exhibited velocities ranging from 0.3 to 5 cm yr^{-1} (Fig. 4 and 5), and were classified into
314 three velocity classes: 0.3 – 1 cm yr^{-1} , 1 – 3 cm yr^{-1} , and 3 – 10 cm yr^{-1} . The measured displacement between 2015 and 2021
315 remained consistent for most MAs, with no significant changes in velocity during this period (see trendlines in Fig. 5). Due to
316 the relatively low velocities of the MAs, tracking seasonal variations involved high uncertainty; therefore, we referred only to
317 annual or multiannual displacement rates.

318 A total of 92 MAs covering 0.27 km^2 were inventoried in the Retezat Mountains rock glaciers. Most of the MAs are classified
319 with the slow velocity class (0.3 – 1 cm yr^{-1} and 1–3 cm yr^{-1}) (Fig. 6), while only 10 % of the MAs are characterised by velocity
320 class 3–10 cm yr^{-1} (Fig. 6a). Around one-third (37 %) of the total number of rock glaciers in the Retezat Mountains contains
321 MAs, but the analysis revealed they usually occupy only a small portion (< 30 %) of the total surface of each rock glacier; in

322 six cases, the cumulated area of MAs represents more than 50 % of the rock glacier area (Fig. 6d). The mean area of MAs is
 323 0.3 ha, ranging from 0.1 to 1.77 ha.
 324 The number of MAs in each rock glacier varies between 1 and 8, but in most cases (69 %), 1 to 3 MAs occur in an individual
 325 RG. MAs characterised by velocities $> 3 \text{ cm yr}^{-1}$ were identified in 8 rock glaciers, whereas MAs classified in the velocity
 326 class $1\text{--}3 \text{ cm yr}^{-1}$ appear in 17 (Fig. 6c).
 327 The median elevation for each MA class falls between 1950 and 2295 m (Fig. 7). Specifically, 62 % of the MAs are found in
 328 the elevation band of 2100 to 2200 m, while 17 % lie between 2200 and 2295 m. Additionally, 16 % of the moving areas are
 329 situated in the range of 2000 to 2100 m, and only 5 % are below 2000 m. Among these, MAs categorised under velocity classes
 330 of $1\text{--}3$ and $3\text{--}10 \text{ cm yr}^{-1}$ generally occur at the highest elevations (Fig. 7a). Figure 7b illustrates the variability of slopes across
 331 the MAs velocity classes, revealing mean values ranging from 8 to 42° . The widest range of slopes is observed in the velocity
 332 class $0.3\text{--}1 \text{ cm yr}^{-1}$, which also exhibits higher median values. Half of the MAs (50 %) face north (Fig. 8), despite that only
 333 21 % of the inventoried rock glaciers in the Retezat Mountains stand out on the northern aspects. The NE and E slopes host
 334 more MAs (32 %) compared to NW and W aspects (23 %) in respect with the rock glacier distribution (Fig. 8). Across the
 335 mountain range, slopes with a western aspect dominate in terms of surface coverage. The MAs with velocities exceeding 3 cm
 336 yr^{-1} receive the lowest potential solar radiation (Fig. 7c).



337
 338 **Figure 4: Example of moving areas and rock glacier activity for the Retezat Mountains. The two RGs are marked with numbers 1**
 339 **and 2 in fig.1. Background image: hillshade based on the LAKI II DEM (LAKI II MNT, 2024).**

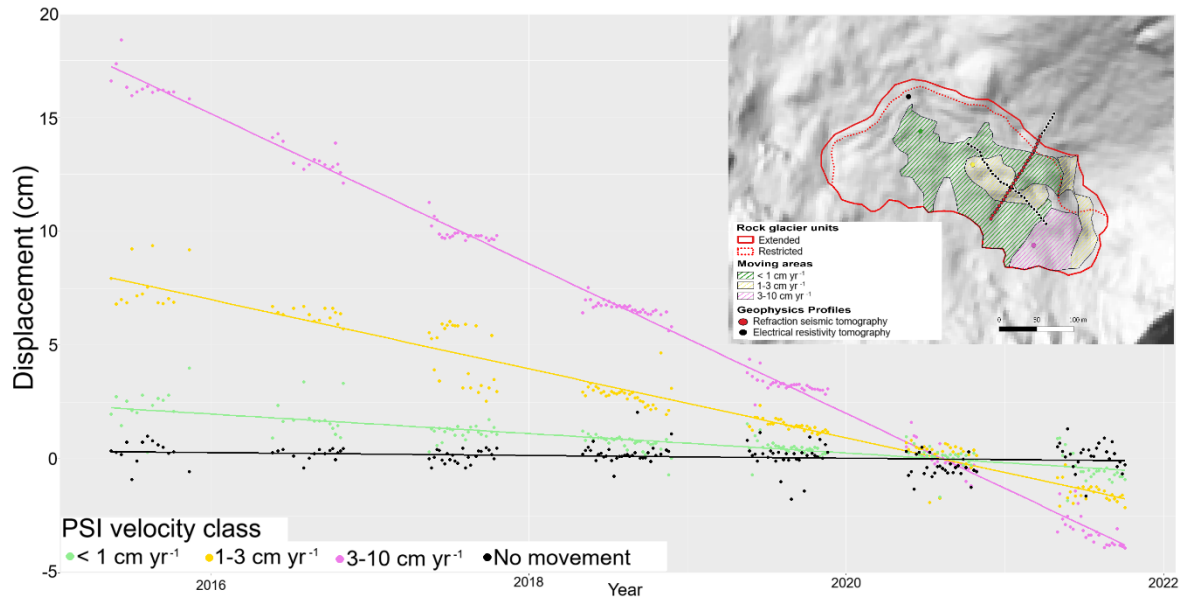


Figure 5: Displacement profiles over a period of 6 years (2015 – 2021) for 4 locations (identified in the location map with dots of corresponding colour) representing each velocity class and one for an area with no movement. The dots show the actual PSI displacement results, while trend lines (linear regressions) indicate long-term motion patterns. The displacement is measured relative to 2021. The downward trend can be interpreted as movement away from the sensor, which in our case represents a combination of vertical movement and horizontal downslope movement. The gap in point density along the trend line is due to the winter season, the measurements being performed in snow free conditions, usually from June to November.

For rock glaciers exhibiting no or minimal movement ($< 1 \text{ cm yr}^{-1}$), the RGIK (2023a), recommends assigning a relict activity class. The present analysis shows that only 21 % of the rock glaciers in the Retezat Mountains could be classified as transitional (Fig. 9a), encompassing areas with moving velocities ranging between 1 and 5 cm yr^{-1} . The transitional rock glaciers exhibit a median elevation of 2170 m, surpassing that of the relict ones by 150 m (Fig. 9b). Additionally, the median size of transitional rock glaciers is slightly smaller than that of relict rock glaciers (Fig. 9c).

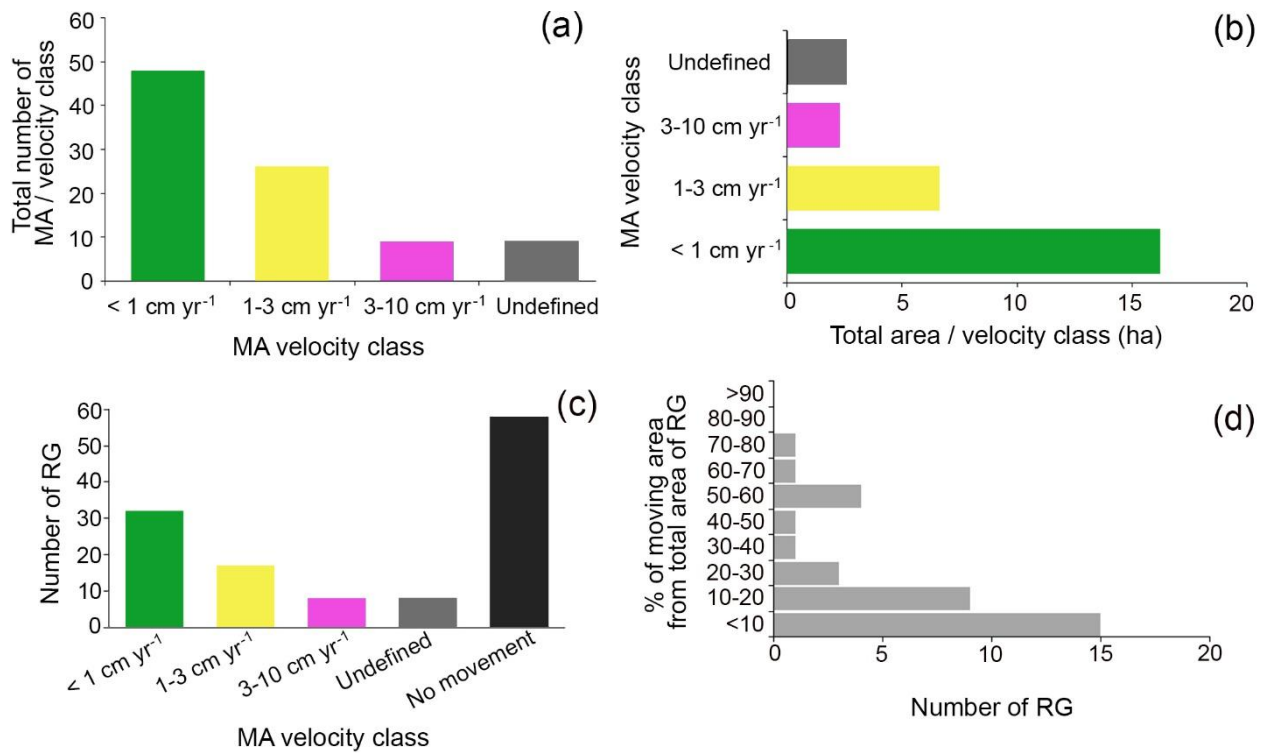


Figure 6: The moving areas classified by velocity classes (a) and their extent (b). The number of rock glaciers containing moving areas and without moving areas (c) and the percentage of the moving area cover within rock glaciers (d).

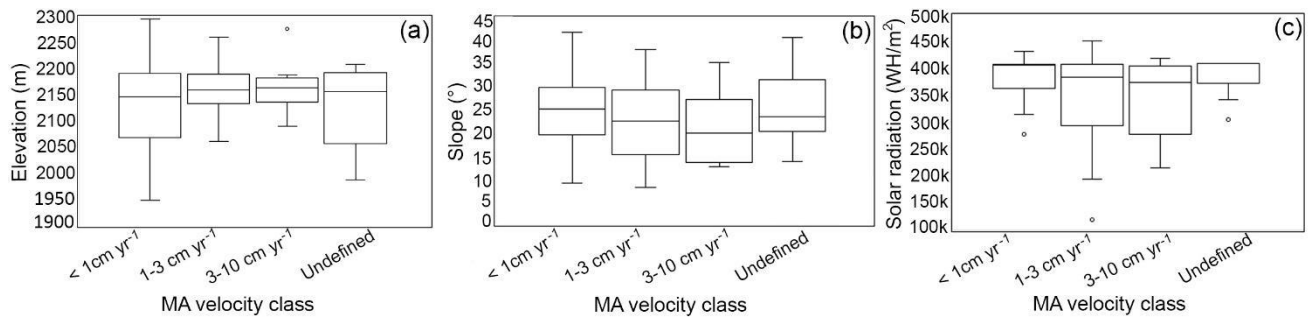


Figure 7: Elevation (a), Slope (b) Potential solar radiation (c) vs MA velocity classes

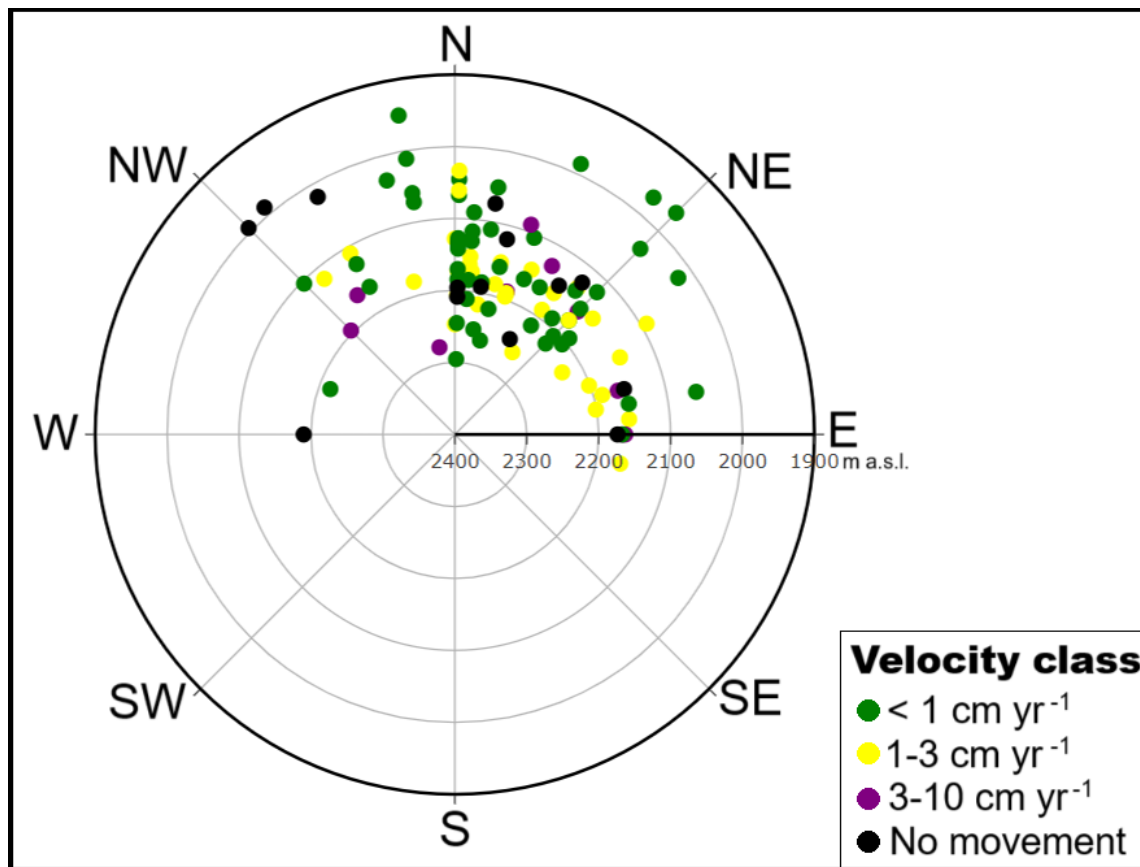


Figure 8: Distribution of moving areas, in the Retezat Mountains, in relation to slope aspect (angular axis) and elevation (radial axis).

Figure 10 presents a comparison between ALOS-2 PALSAR-2 interferogram and the Sentinel-1 PSInSAR results at Galeşu (7) site. Although the accuracy of the ALOS-2 PALSAR-2 is lower, both products exhibit similar signals. The main displacement areas are clearly visible and coincide on both maps

The comparison between PSI and InSAR performance reveals that, in areas with high variability in displacement, PSI provides more detailed mapping of the monitoring areas (MAs), allowing for the differentiation of relatively minor velocity differences. In Fig. 10b, a specific MA is clearly identified and classified as having a velocity of $<1 \text{ cm yr}^{-1}$. The same area appears in Fig. 10a, where most of it is also mapped as $<1 \text{ cm yr}^{-1}$; however, adjacent zones are classified as $1\text{--}3 \text{ cm yr}^{-1}$ and $3\text{--}10 \text{ cm yr}^{-1}$, indicating a broader range of detected velocities.

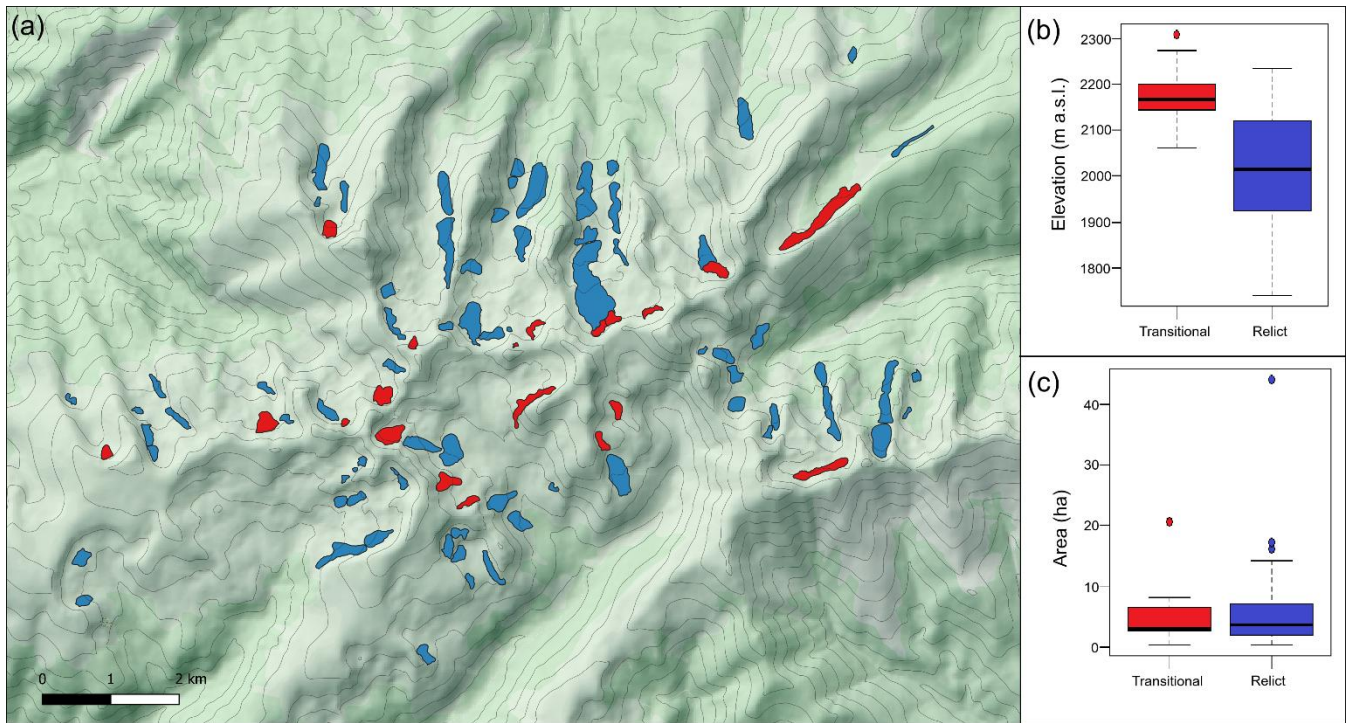


Figure 9: The spatial distribution of transitional and relict rock glaciers in the Retezat Mountains (a) and their median elevation (b) and size (c).

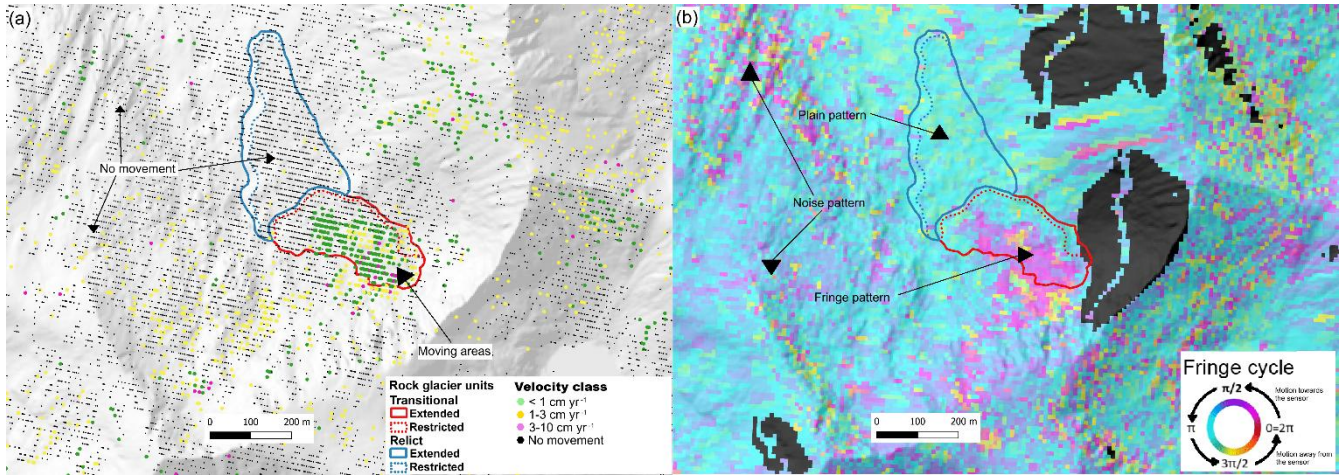
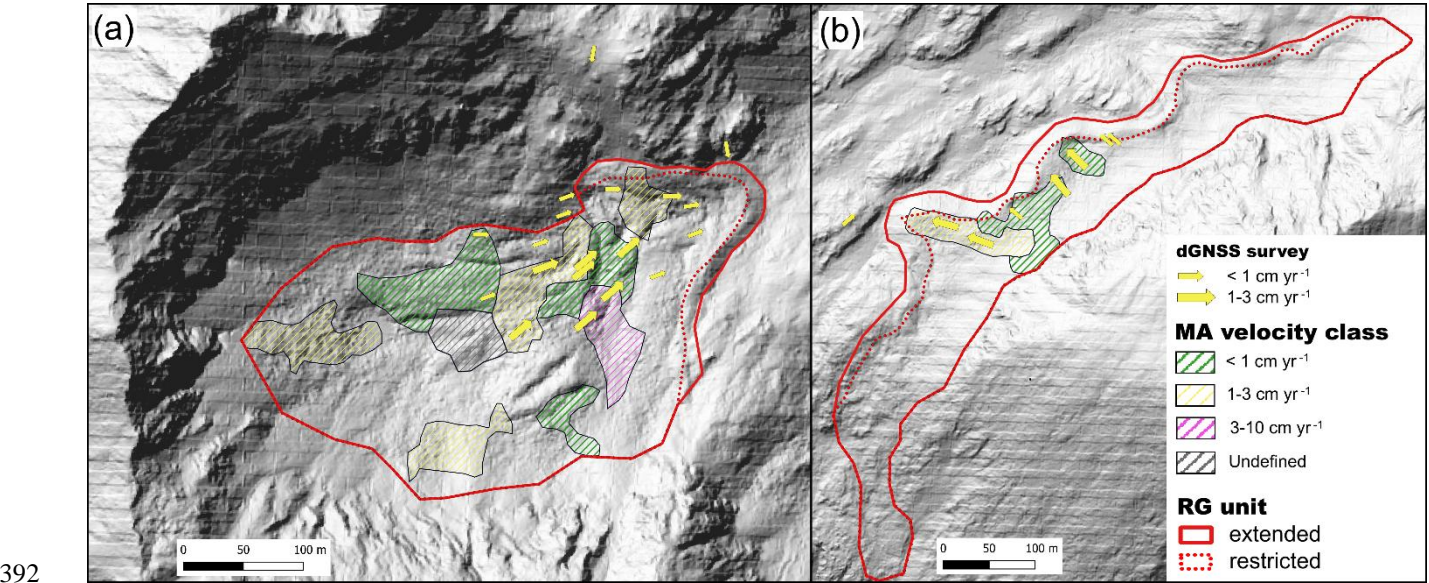


Figure 10: A comparison between multiannual PSINSAR from Sentinel 1 (a) and InSAR from ALOS-2 PALSAR-2 (b). Notice the same moving areas inside the RGs, that are revealed by clustered pixels with movement (green, yellow and magenta) from PINSAR (a) and the areas with fringe patterns (b). In (b) the shadow areas are masked out and the fringe cycle (bottom right) represents the change of colour. Fig. 10b presents the Galeşu RG where in the upper RGU we have one fringe over a five year period (September 2014 to October 2019) accounting for a displacement of approximately 0.56 cm/yr. This is in line with the PSI measurements that have the biggest MA on the RG to be <1 cm/yr.

379 **4.2. GNSS measurements**

380 The mean velocities measured by dGNSS ranged between 0.4 and 2.8 cm yr⁻¹, with values exceeding 1 cm yr⁻¹ for 56 % of the
381 marker points (Fig. 11). On the Judele (8) rock glacier, eight marker points recorded velocities between 1 and 2.6 cm yr⁻¹,
382 while nine points showed velocities between 0.4 and 1 cm yr⁻¹. The highest velocities are observed in the central part, gradually
383 decreasing toward the margins. One marker point measured on the front of Judele rock glacier revealed very low rates of
384 displacements (0.4 cm yr⁻¹). Almost all marker points indicate consistent movement toward the front of the rock glacier. Four
385 marker points on the Berbecilor (9) rock glacier revealed velocities between 1 and 2.8 cm yr⁻¹ and three between 0.6 and 1 cm
386 yr⁻¹. All the seven marker points indicate consistent movement toward the front. Most marker points with moving velocities
387 between 1 and 2.8 cm yr⁻¹ (89 %) were located within MAs categorised under the 1-3 and 3-10 cm yr⁻¹ velocity classes by
388 PSInSAR analysis. At Judele, five out of eight dGNSS markers recording velocities between 1 and 2.6 cm yr⁻¹, fall within the
389 1-3 cm yr⁻¹ velocity class, whereas at Berbecilor the ratio is two out of four. At both sites, nine marker points with velocities
390 between 0.4 and 1 cm yr⁻¹ are located outside any designated MAs, while only three falls within the corresponding velocity
391 class.

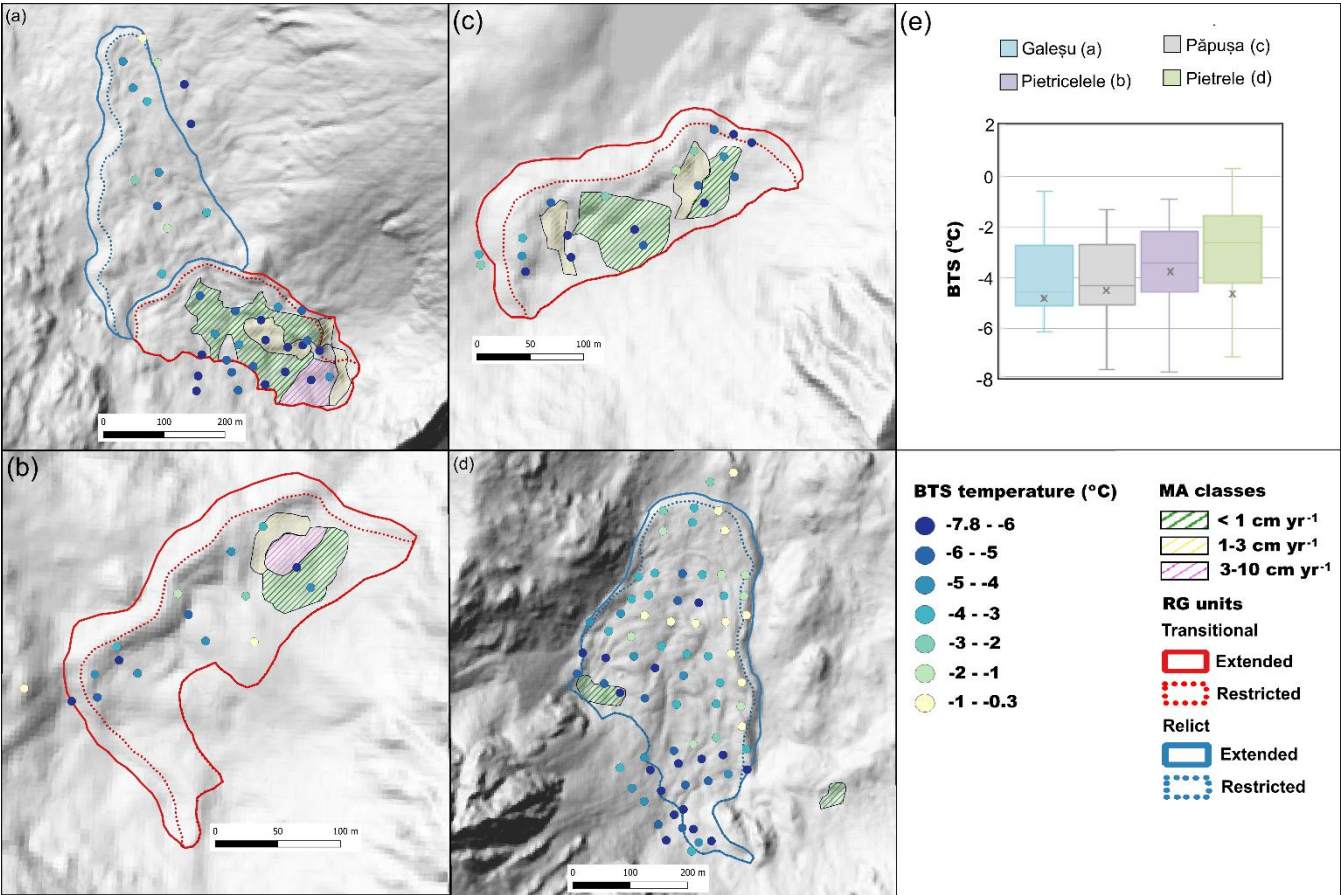


393 **Figure 11: Horizontal displacements derived from GNSS measurements for 2019-2021 at Judele (a) and Berbecilor (b) sites,**
394 **overlayed on the MAs derived from PSInSAR. Background of both maps: hillshade based on the LAKE II DEM (LAKE II MNT,**
395 **2024)**

396 **4.3. BTS and ground temperatures**

397 BTS measurements allowed the identification of colder versus warmer ground surface areas in four rock glaciers (Fig. 12).
398 Half of the 140 measured BTS points were measured on Pietrele (3) rock glacier, which has the lowest front altitude and
399 revealed the warmest mean of BTS values (-2.9 °C). The coldest temperatures at this site occurred in the uppermost part, where

400 most BTS values were below $-3\text{ }^{\circ}\text{C}$. Several BTS points measured on the talus slope feeding this rock glacier also revealed
 401 very low temperatures. In the western part, where a MA in the $0.3\text{-}1\text{ cm yr}^{-1}$ velocity class is present, BTS values consistently
 402 fell below $-5\text{ }^{\circ}\text{C}$. At the Galeşu multi-unit rock glacier, the mean BTS was $-3.9\text{ }^{\circ}\text{C}$, with the coldest values clustered in the
 403 southern unit and on the upslope talus. The BTS values within the MAs were all very low, below $-5\text{ }^{\circ}\text{C}$. In contrast, the northern
 404 rock glacier unit, which showed no signs of surface displacement, exhibited a highly heterogeneous distribution of BTS values.
 405 Păpuşa (6) is the highest rock glacier where BTS measurements were performed and revealed the lowest average of BTS values
 406 (-4.1°C), whereas at Pietricelele (4), the mean BTS was $-3.5\text{ }^{\circ}\text{C}$. At Păpuşa site, a warmer zone occurred in the central part,
 407 with three BTS values warmer than $-2\text{ }^{\circ}\text{C}$; however, all BTS values within the MAs indicated very cold ground conditions
 408 Similarly, at Pietricelele, a warmer ground surface area was identified in the central and northeastern parts, while the western
 409 and southeastern areas revealed colder temperatures. Snow depth at the probing points ranged from 80 and 260 cm. In all the
 410 cases, the calculated median BTS in MAs was lower compared with the median of all BTS values in each site.



411
 412 **Figure 12: BTS measurements performed in March 2022 on four rock glaciers in the Retezat Mountains: (a) Galeşu, (b) Pietricelele,**
 413 **(c) Păpuşa, (d) Pietrele. (e) Summary box-plot diagram of the BTS measurements, the horizontal line drawn inside denotes the**
 414 **median BTS for each rock glacier, while the x represents the median BTS of the moving areas of each rock glacier). (f) the legend**
 415 **for the maps in (a), (b), (c) and (d).**

416 In most cases, MAGST values were negative at the monitoring sites from 2013 to 2022, ranging from -2.3 °C to 0.8 °C, with
417 the lowest values recorded at Galeșu and the highest at Pietrele. To illustrate long-term GST evolution, Figure 13a shows the
418 running annual mean of ground surface temperature. However, subzero MAGST values were recorded only at site Valea Rea
419 (5) in all the years, whereas at Galeșu, all the MAGST values were below 0 °C except one year (e.g., 2016). All the GST sites
420 revealed negative values for the mean temperature of the entire monitoring interval.

421 Fig. 13c reveals the mean daily temperature at the GST monitoring sites. The lowest GST values (< -10 °C) occurred in
422 October-December under snow-free or thin snow cover conditions. This is because the insulating snow cover typically occurs
423 in November/December, whereas the snow disappears in May or June. However, at all the sites, significant ground cooling
424 was observed even during the January-March period, despite snow depths typically being sufficient to insulate the ground from
425 air temperature fluctuations. For example, at Galeșu, almost every winter exhibited notable short-term fluctuations in the GST
426 regime. Similar, through less pronounced, patterns were also observed at Judele (e.g., winters of 2013-2014 and 2017-2018),
427 Pietrele (e.g., 2012-2013, 2013-2014, 2014-2015, 2016-2017 and 2021-2022) and Valea Rea (e.g., 2015-2016 and 2019-2020).
428 In a few instances, inverse thermal relationships between ground surface temperature and air temperature were recorded,
429 confirming the presence of internal ventilation through the coarse debris during winter. These thermal anomalies are likely
430 driven by advective heat fluxes that remain active beneath thick snow cover and likely contribute to the cold MAGST observed
431 in the rock glaciers. Usually, during March, ground surface temperatures are relatively stable and are mainly driven by
432 conductive processes. In almost all cases, the corresponding WEqT were below -2 °C, indicating possible or probable
433 permafrost occurrence (Fig. 13b). WEqT values higher than -2 °C occurred only at Pietrele in late winter 2013 and 2014. At
434 Valea Rea and Judele, most WEqT values were between -2 and -3 °C, whereas at Galeșu, the late winter temperatures were
435 considerably lower.

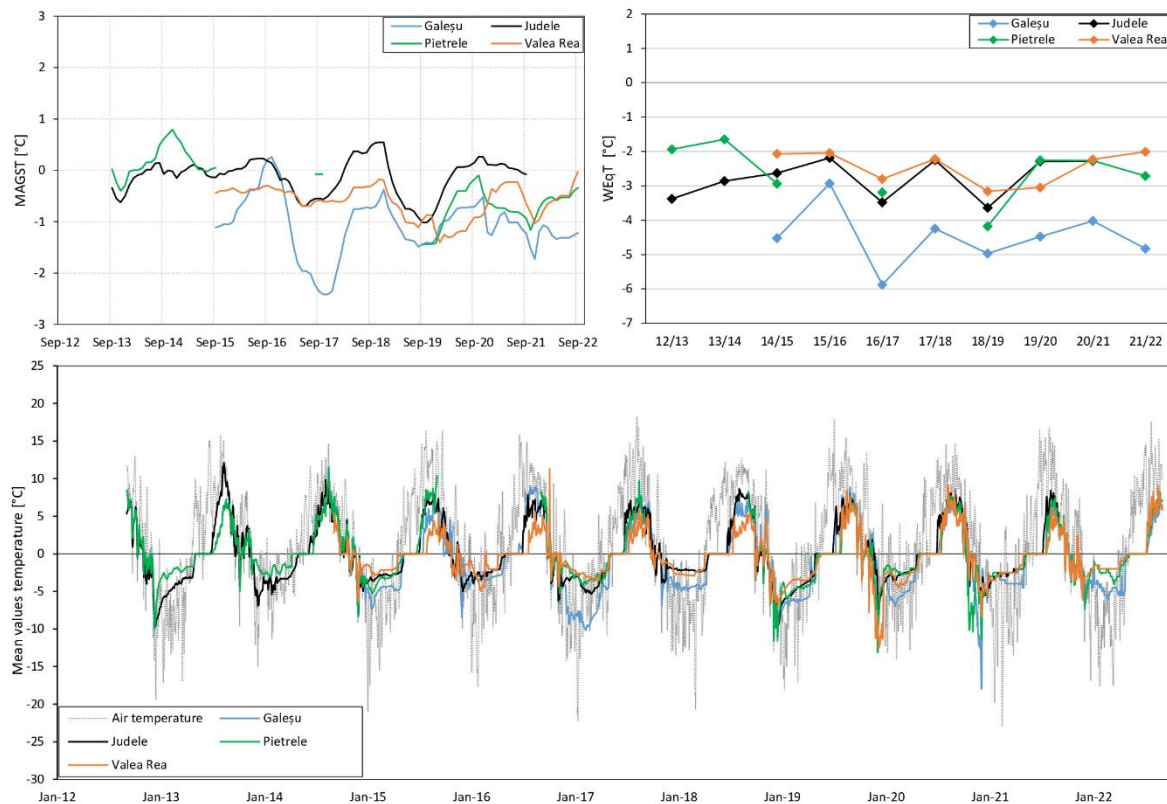


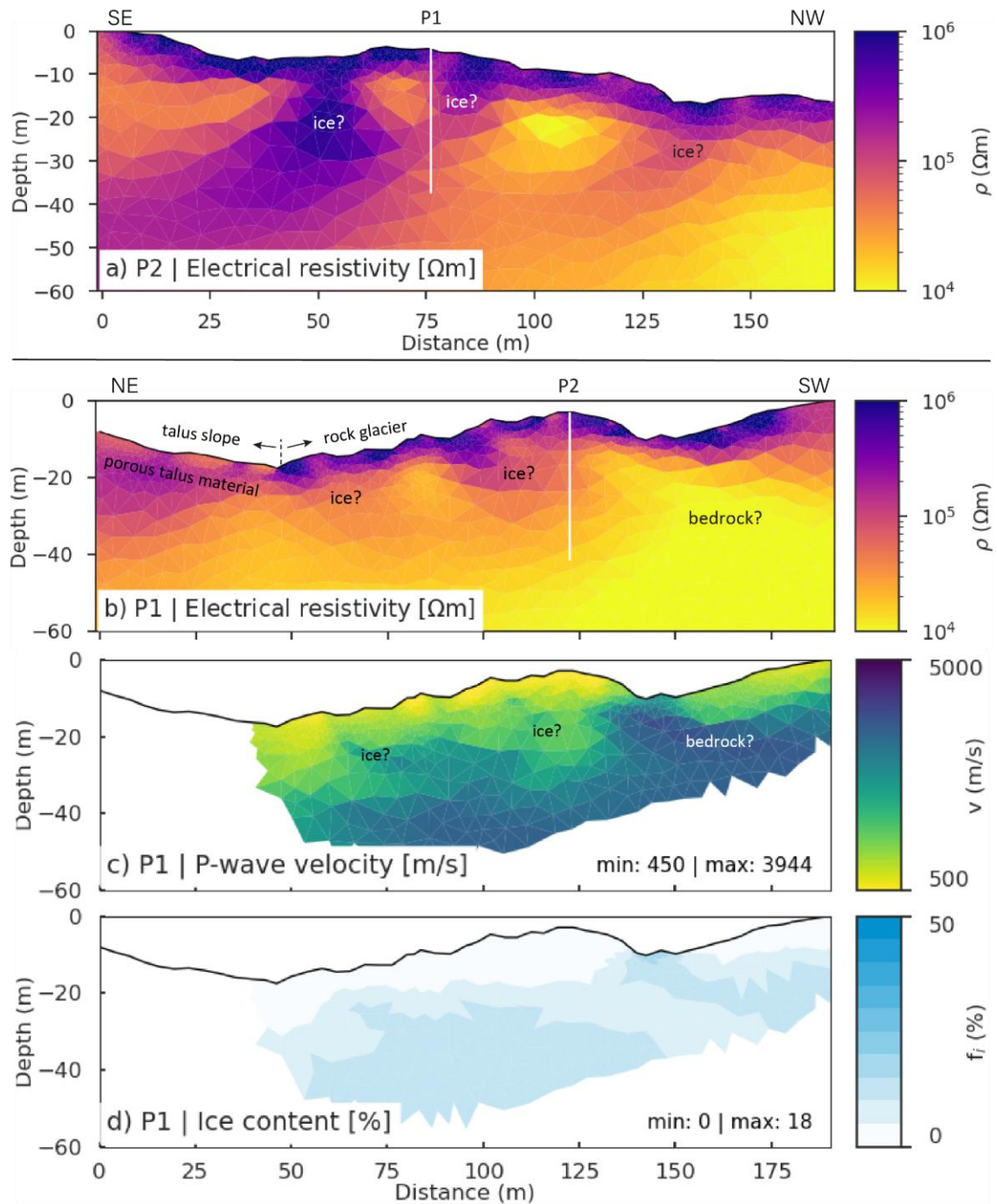
Figure 13: (a) Running 12-month average of mean annual ground surface temperature, (b) Winter Equilibrium Temperature (WEqT) and (c) Running 12 months average of Ground Surface Temperature (GST) for the period 2012/2013 to 2021/2022 at four sites in the Retezat Mountains and air temperature at Țarcu meteorological station (2180 m).

4.4. Geophysics results

The results of the geophysical surveys at Galeşu rock glacier are shown in Figure 14 for the two crossing ERT profiles P1 and P2 (Fig. 14a, b), as well as the RST and PJI results available for profile P1 (Fig. 14c, d). Both ERT tomograms reveal an up to 5 m thick layer characterised by high resistivities ($> 200 \text{ k}\Omega\text{m}$) representing the dry and coarse-blocky surface layer. Patchy occurrences with similarly high resistivities are observed in 5-20 m depth in both profiles, which could indicate remnants of former ice-rich permafrost within the rock glacier (labelled with 'ice?' in Fig. 14). Below, a more homogeneous layer of resistivities around $10 - 30 \text{ k}\Omega\text{m}$ may indicate the rock glacier base (bedrock) in the southwestern part of profile P1, however, the resistivity values do not exclude the possibility of frozen conditions and the interpretations of this zone remains ambiguous. The landform's overall thickness is estimated at $< 20 - 30 \text{ m}$ and potentially $< 15 \text{ m}$ in the southwestern part of profile P1. The eastern part of profile P1 ($x < 50 \text{ m}$ in Fig. 14b) is located outside the rock glacier and traverses into a partially vegetated talus slope. Here, the surface layer exhibits lower resistivities ($< 100 \text{ k}\Omega\text{m}$, probably representing smaller block size and organic material), and the underlying resistive layer ($100\text{-}200 \text{ k}\Omega\text{m}$) has a thickness of about 10 m and a more homogeneous appearance

452 than that of the rock glacier. Both the morphology and the resistivity values point to a potentially frozen ventilated talus slope,
453 but this is not a focus of this study and will not further be explored.

454



455

Figure 14: a) and b) ERT profiles P2 and P1 (see Fig. 1c for location), c) RST profile, and d) modelled ground ice content based on the PJI.

The seismic profile P1 (Fig. 14c) only covers the rock glacier part of the ERT profile P1 and shows a 5-10 m thick upper layer with P-wave velocities $< 1500 \text{ m s}^{-1}$, indicating highly porous blocky material. The velocities are increasing with depth, reaching 4000 m s^{-1} at about 20-25 m depth in the central part of the rock glacier and at shallower depths ($\sim 15 \text{ m}$) in the last 50 m of the profile. According to the seismic data, ice-rich permafrost would be possible in large parts of the tomogram. However, in combination with the ERT data, ice-rich conditions seem only plausible in those parts of the tomogram that coincide with elevated resistivities. Alternatively, the zones with lower resistivities could also indicate zones with increased conductivity due to ongoing ice melt, the interpretation therefore remains ambiguous. The seismic data further indicate relatively porous material rather than firm bedrock and point to an overall larger thickness of the rock glacier than indicated by the ERT profile.

The result of the PJI modelling (Fig. 14d) reveals a generally very low ground ice content in the upper sector of the Galeşu rock glacier, with maximum values of 18 %. The highest ice contents coincide with zones with highest seismic velocity, partly contradicting the individual interpretation (bedrock). This can be due to the known rock-ice ambiguity of the current PJI formulation, as the rock and ice content are only directly constrained through the petrophysical equation of the seismic velocity. As a consequence, the correct differentiation between rock and ice is problematic in some cases (see Mollaret et al., 2020 for details). The generally low ice contents modelled through the PJI therefore mainly confirm that a potential former massive ice core is not detectable anymore and point to an advanced state of degradation of this rock glacier. However, these results do not exclude the possibility of more confined ice-saturated or even supersaturated layers (as expected based on the analysis of InSAR data in section). Due to the limited resolution capacity of the geophysical profiles with 4 m sensor spacing thin ice-rich or ice-supersaturated layers may not be resolvable as such, but - depending on their depth and extent - with strongly reduced spatial gradients of the ice content (as well as resistivity or velocity contrast in the individual tomograms). The relatively homogeneous ice content distribution modelled from the PJI may therefore not only reflect the rock-ice ambiguity mentioned above, but also this limitation to resolve small-scale structures.

5. Discussion

5.1. Assessing the velocity of rock glaciers in marginal periglacial environments

In marginal periglacial regions rock glaciers exhibit a minimal rate of motion (a few cm yr^{-1}) (Necsoiu et al., 2016) and evaluating their velocity can pose occasional challenges. Hence, the compilation of MAs inventory might be affected by limitations associated with radar interferometry (Bertone et al., 2022).

The PSInSAR measurements were provided in the SAR LOS direction, representing a 1-D rather than a 3-D measurement, capturing only a single component of motion. Due to the particular steep topography of the study area, it can be assumed that

the movement direction of the actual motion is oriented along the mountain slope. Although PSInSAR does not produce the exact 3-D velocity vectors, this work was helpful in detecting areas of motion and refining the rock glaciers inventory. Slow-moving areas (i.e., 0.3-1 cm yr⁻¹; 1-3 cm yr⁻¹) are prevalent in this region, where only 10% of the MAs are characterised by velocities exceeding 3 cm yr⁻¹. The latter tend to occupy higher elevations and receive less solar radiation than slower ones. Overall, the median size of the MAs from Retezat Mountains is slightly smaller than other periglacial environments (Bertone et al., 2022). The median size of the MAs, showing minimal variation across velocity classes, exhibits a slight peak among those moving at < 1 cm yr⁻¹ (0.33 ha). The median size of MA velocity classes of 1-3 cm yr⁻¹ and 3-10 cm yr⁻¹ is 0.3 ha, roughly one-third smaller than those reported in Southern Tyrol (Bertone et al., 2024).

The examination of displacement measurements through the differential GNSS technique unveiled similarly very slow movements at specific points (ranging from a few millimetres to 2.8 cm yr⁻¹). A comparison between the GNSS survey and PSInSAR results revealed that there was not a very good correspondence between these outcomes. The discrepancy may be due to the difficulty both methods have in accurately detecting such slow movement. Additionally, differences between the velocity datasets may result from the distinct time intervals used for analysis - 2015-2021 for PSInSAR and 2019-2021 for dGNSS. However, most GNSS survey markers that exhibited horizontal displacements exceeding 1 cm yr⁻¹ were still located within the MAs. In terms of flow direction, the majority of these markers indicated consistent movement toward the fronts of Judele and Berbecilor rock glaciers, behavior characteristic of permafrost creep.

The PSInSAR analysis enriches the existing rock glacier inventory with information about the activity status of rock glaciers in the Retezat Mountains. A previous study classified 30 rock glaciers in the study area as intact based on geomorphological and ecological criteria (Onaca et al., 2017b). Radar interferometry revealed that 20 rock glaciers exhibit surface displacements exceeding 1 cm yr⁻¹. In contrast, 15 rock glaciers showed minimal displacements (0.3 – 1 cm yr⁻¹). Of these, eight were previously classified as intact, while the remaining seven were categorised as relict. Four rock glaciers, previously labelled as geomorphologically relict, show surface displacements exceeding 1 cm yr⁻¹ and were categorised as transitional in our study. Unlike other regions (e.g., Central Italian Alps, Eastern European Alps, Himalaya) where there is a considerable elevation difference between active/intact and relict rock glaciers (Kellerer-Pirklbauer et al., 2012; Scotti et al., 2013), the Retezat Mountains exhibit a significantly smaller separation.

5.2. Permafrost occurrence revealed by geophysical and temperature measurements

The geophysical investigations revealed a frozen layer with overall low ice contents beneath a substantial active layer of approximately 5 m thickness. Similar results have been reported in other marginal periglacial environments (i.e., Făgăraș Mountains, Pirin Mountains, Italian Carnic Alps) where thick active layers indicate even greater thickness (Onaca et al., 2013; Colucci et al., 2019; Onaca et al., 2020). Due to the rock glacier's very dry and extremely coarse blocky surface, the ERT data only have limited quality which is also reflected by the high resistivities of > 200 kΩm on the rock glacier surface. However, we still assume that the overall resistivity pattern indicates the main structures and is representative for the site, whereas small-scale anomalies present in the tomograms as well as absolute resistivity values, should be interpreted with care.

The BTS measurements revealed very cold surface temperatures across large portions of the rock glaciers, with particularly low values observed within MAs, in the upper sections of the rock glaciers, and along the upper talus slopes. However, not all cold areas exhibited detectable movement in the PSInSAR results. Conversely, considerably warmer ground surface temperatures were also recorded in various parts of the rock glaciers, supporting the presence of internal ventilation. The GST results suggest favourable conditions for permafrost existence, but more notably highlight significant ground cooling episodes during the winter, likely driven by air advection. Similar results have been reported for Judele, Pietrele, Valea Rea, Galeșu and Pietricelele rock glaciers in previous studies (Vespremeanu-Stroe et al., 2012; Onaca et al., 2015). Except for Pietrele, the other data-logger sites (Galeșu, Judele and Valea Rea) are located in areas with displacement velocities exceeding 1 cm yr⁻¹. However, at Pietrele, despite the prevalence of low BTS values, almost no displacement was observed, except in the western part, where minor displacements (0.3 – 1 cm yr⁻¹) were detected. The Pietrele rock glacier is oriented along a south-north direction and the LOS orientation tends to underestimate displacements on north facing slopes (Liu et al., 2013). The lack of significant displacement in this rock glacier between 2014 and 2021 does not necessarily indicate complete ice melt, but likely suggests negligible ice content.

5.3. Rock glaciers behaviour in marginal periglacial environment

The rock glaciers in the Southern Carpathians generally move at slower rates than those in other mid-latitude high mountains, where rock glaciers' velocities range from a few centimetres to a few meters per year. But rock glaciers experiencing very low movement velocities were also documented in different periglacial regions (e.g., Pyrenees, Rocky Mountains, northern Norway, Southern Alps of New Zealand, etc.) (Serrano et al., 2010; Brencher et al., 2021; Rouyet et al., 2021; Bertone et al., 2022; Lambiel et al., 2023). In the Retezat Mountains, only 21 % of the inventoried rock glaciers display motion, whereas the rest are considered relict. Similar to the Uinta Mountains (Brencher et al., 2021), in most cases, only a relatively reduced portion of the rock glacier exhibits movements. An illustrative case in this regard is the Galeșu multi-unit rock glacier, displaying movement solely in its uppermost unit, where a younger lobe overlies the main body of the rock glacier. Similar younger lobes were identified in other valleys (e.g., Valea Rea, Pietrele) representing distinct phases of rock glaciers activity, as observed in many other periglacial regions of Europe (e.g. Iceland, European Alps, Cantabrian Mountains, Pyrenees etc.) (Farbrot et al., 2007; Kellerer-Pirklbauer et al., 2008; Steinemann et al., 2020; Amschwand et al., 2021; Oliva et al., 2021; Santos-González et al., 2022).

Additionally, the PSInSAR analysis revealed that, in many instances, the fronts of the rock glaciers in the Retezat Mountains remain stable. Notable examples of stable fronts include Judele (Fig. 11a), Berbecilor (Fig. 11b), Galeșu (Fig. 12a), Păpușa (Fig. 12c) and Pietricelele (Fig. 12b). Field observations also confirmed that despite steep and sometimes unvegetated slopes, the rock glacier fronts display no recent activity, and no ploughed grass occurs at their snouts. This type of rock glacier, called climatically inactive (Barsch, 1996), is also distinguished by a substantial unfrozen mantle and a low ice content (Onaca et al., 2013).

553 The geophysical measurements performed in this study indicated the very low ice content in the Galeșu rock glacier,
 554 insufficient to support permafrost creep. For permafrost creep to occur, frozen conditions must extend to a depth of at least 10-
 555 25 m (Cicoira et al., 2021), which does not appear to be the case at Galeșu. Surface displacements at this site are more likely
 556 the result of ice-melt-induced subsidence, solifluction, or the tilting and sliding of blocks within the active layer. In contrast,
 557 the flow direction of dGNSS markers at Judele and Berbecilor showed consistent movement patterns, which are not typical of
 558 ice-melt subsidence or any other active-layer processes. Additional geophysical and dGNSS measurements are needed to better
 559 distinguish between these mechanisms in marginal periglacial environments.

560 Various studies suggest that the volumetric ice content within active rock glaciers typically falls within the range of 40 % to
 561 60 % (Barsch, 1996; Hausmann et al., 2007; Rangecroft et al., 2015). Conversely, for rock glaciers tending towards inactivity,
 562 Wagner et al. (2021) propose average ice content as low as 20 %. These estimates are commonly used to assess the water
 563 volume equivalent of ice content stored in rock glaciers (Wagner et al., 2021; Pandey et al., 2024). However, the geophysical
 564 investigations presented in this paper reveal even lower values for the volumetric ice content of the Galeșu rock glacier. This
 565 finding suggests that the ice content in transitional rock glaciers may be considerably lower than expected, emphasising caution
 566 when calculating water volume equivalent on a broad scale.

567 Considering the current MAGST of approximately -0.5 °C and assuming a climatic warming of about +1.5 °C since the late
 568 19th century (Allen et al., 2018), it is likely that these rock glaciers had a MAGST around -2 °C during the pre-industrial period.
 569 At such low temperatures, widespread permafrost conditions would have been expected, and the presence of deep permafrost
 570 cannot be ruled out. However, accelerated warming in recent decades has resulted in permafrost warming, particularly in ice-
 571 poor bedrock, at rates comparable to the increase in air temperature (Noetzli et al., 2024). BTS measurements and GST patterns
 572 observed during winter suggest ongoing convective and advective air flow processes that maintain cold ground conditions and
 573 support the persistence of ice non-saturated permafrost in the Retezat Mountains.

574 The results presented in this study align with the coarse-rock glacier hypothesis (Onaca et al., 2015; Popescu et al., 2017),
 575 which suggests that permafrost occurrence in the Carpathian Mountains is patchy and limited to sites above 2100 m with low
 576 solar radiation. In these locations, very coarse rock glaciers, hosting numerous large boulders, facilitate strong cooling through
 577 internal ventilation (e.g., advection and convection) (Wicky and Hauck, 2017; Amschwand et al., 2024) and air stratification
 578 (low conductivity) during summer or under thick snow cover.

579 **6. Conclusions**

580 This study leads to the following main conclusions:

- 581 - The majority of rock glaciers in the marginal periglacial environment of the Retezat Mountains are classified as relict,
- 582 with only 21% categorized as transitional. The median elevation of transitional rock glaciers is 150 m higher than that of relict
- 583 rock glaciers and their median size is slightly smaller. The PSInSAR methodology enabled the identification of new rock
- 584 glaciers displaying movements, which were initially classified as relict features.

585 - A total of 92 moving areas were delineated within the rock glaciers of the Retezat Mountains, predominantly falling
586 within the slow-velocity classes ($0.3 - 1 \text{ cm yr}^{-1}$ and $1-3 \text{ cm yr}^{-1}$). Moving areas exhibiting velocities between 1 and 5 cm yr^{-1}
587 are typically located above 2100 m in regions with minimal solar radiation income. Higher movement rates are observed in
588 the upper, younger lobes compared to the well-developed lower parts.

589 - Long-term ground temperature monitoring from 2012 to 2022 revealed low MAGST values at the observation sites,
590 ranging from $-2.3 \text{ }^{\circ}\text{C}$ to $0.8 \text{ }^{\circ}\text{C}$. Internal ventilation processes (e.g., advection) occurring throughout the winter significantly
591 contribute to surface cooling and appear to sustain permafrost conditions in coarse debris above 2100 m. This is further
592 supported by BTS measurements, which indicate very cold ground temperatures beneath a thick late-winter snow cover.

593 - Geophysical measurements conducted on an intact rock-glacier revealed notably low ice content (with maximum
594 values of 18%) in its uppermost section. At this site, surface displacements are most likely driven by processes such as ice-
595 melt-induced subsidence, solifluction or blocks sliding. In contrast, the consistent flow of dGNSS markers towards the fronts
596 of the Judele and Berbecilor rock glaciers points to permafrost creep.

597 Our findings highlight the value of combining Sentinel-1 SAR data with extensive field investigation (such as DGPS,
598 geophysical and thermal methods) and where possible, with other remote sensing data (like ALOS-2 PALSAR-2), particularly
599 in regions with slow-moving rock glaciers. This approach could serve as a benchmark for similar studies in marginal periglacial
600 environments.

601 **Code/Data availability**

602 The deformation data, obtained using PSI, and the temperature data, obtained using GST data loggers and BTS are freely
603 available as a Zendo repository, at <https://zenodo.org/records/14544941>, DOI: 10.5281/zenodo.14544940

604 For further questions about data processing readers are encouraged to contact the authors.

605 **Author Contribution**

606 The study was conceptualized and managed by AO and FS. AO led the manuscript writing, with contributions from VP, CH,
607 PU, TS and FS. VP, TS, DT, DB and FS contributed to the PSInSAR analysis. FA and IL produced the inventory of moving
608 areas and performed the statistical analysis related to rock glaciers. AO, OB, RP, MV, IL and AVS contributed to the analysis
609 of thermal measurements. CH, BE, SF, RP and AO were involved in conducting and analysing the geophysical measurements.
610 AH and AO provided the GNSS measurements. All authors provided feedback on the final version of the paper.

611 **Competing interests**

612 The authors declare that they have no conflict of interest.

613 Acknowledgements

614 This research was funded by the ESA Permafrost_CCI project (grant number 4000123681/18/I-NB), EEA Norway Grants
615 2014–2021, under project code RO-NO-2019-0415 / contract no. 302020 and PNRR-III-C9 2022 - I8, CF 253/29.11.2022,
616 760055/23.05.2023. We would also like to thank Sabina Calisevici, Adrian C. Ardelean, Patrick Chiroiu, Trond Eiken,
617 Romolus Mălăieștean, Ilie Adrian and Fabian Timofte for support in the fieldwork.

618 References

619 Allen, M. R., Dube, O. P., Solecki, W., Aragón-Durand, F., Cramer, W., Humphreys, S., Kainuma, M., Kala, J., Mahowald,
620 N., Mulugetta, Y., Perez, R., Wairiu, M., and Zickfeld, K.: Framing and Context, In: Global Warming of 1.5 °C, In: An IPCC
621 Special Report on the impacts of global warming of 1.5 °C above pre-industrial levels and related global greenhouse gas
622 emission pathways, in the context of strengthening the global response to the threat of climate change, edited by: Masson-
623 Delmotte, V., Zhai, P., Pörtner, H.-O., Roberts, D., Skea, J., Shukla, P. R., Pirani, A., Moufouma-Okia, W., Péan, C., Pidcock,
624 R., Connors, S., Matthews, J. B. R., Chen, Y., Zhou, X., Gomis, M. I., Lonnoy, E., Maycock, T., Tignor, M., and Waterfield,
625 T., Cambridge University Press, Cambridge, UK and New York, NY, USA, pp. 49–
626 92, <https://doi.org/10.1017/9781009157940.003>, 2018.

627 Amschwand, D., Ivy-Ochs, S., Frehner, M., Steinemann, O., Christl, M., and Vockenhuber, C.: Deciphering the evolution of
628 the Bleis Marscha rock glacier (Val d'Err, eastern Switzerland) with cosmogenic nuclide exposure dating, aerial image
629 correlation, and finite element modeling, *The Cryosphere*, 15, 2057–2081, <https://doi.org/10.5194/tc-15-2057-2021>, 2021.

630 Amschwand, D., Scherler, M., Hoelzle, M., Krummenacher, B., Haberkorn, A., Kienholz, C., and Gubler, H.: Surface heat
631 fluxes at coarse blocky Murtèl rock glacier (Engadine, eastern Swiss Alps), *The Cryosphere*, 18, 2103–2139
632 <https://doi.org/10.5194/tc-18-2103-2024>, 2024.

633 Archie, G. E.: The electrical resistivity log as an aid in determining some reservoir characteristics, *Petroleum Transactions of*
634 *American Institute of Mining and Metallurgical Engineers (AIME)*, 146, 54–62, <https://doi.org/10.2118/942054-G>, 1942.

635 Barboux, C., Delaloye, R., and Lambiel, C.: Inventorying slope movements in an Alpine environment using DInSAR, *Earth*
636 *Surf. Processes*, 39, 2087–2099, <https://doi.org/10.1002/esp.3603>, 2014.

637 Barsch, D.: *Rockglaciers: Indicators for the Present and Former Geoecology in High Mountain Environments*, Springer, Berlin,
638 331 pp, ISBN 3-540-60742-0, 1996.

639 Bernhard, L., Sutter, F., Haeberli, W., Keller, F.: Processes of snow/permafrost-interaction at a high-mountain site,
640 Murtèl/Corvatsch, Easterns Swiss Alps, in 7th International Conference on Permafrost, Yellowknife, Canada, Collection
641 Nordicana, vol. 57, 35–41, 1998.

642 Bertone, A., Barboux, C., Bodin, X., Bolch, T., Brardinoni, F., Caduff, R., Christiansen, H. H., Darrow, M. M., Delaloye, R.,
643 Etzelmüller, B., Humlum, O., Lambiel, C., Lilleøren, K. S., Mair, V., Pellegrinon, G., Rouyet, L., Ruiz, L., and Strozzi, T.:

644 Incorporating InSAR kinematics into rock glacier inventories: insights from 11 regions worldwide, *The Cryosphere* 16, 2769–
645 2792, <https://doi.org/10.5194/tc-16-2769-2022>, 2022.

646 Bertone, A., Jones, N., Mair, V., Scotti, R., Strozzi, T., and Brardinoni, F.: A climate-driven, altitudinal transition in rock
647 glacier dynamics detected through integration of geomorphological mapping and synthetic aperture radar interferometry
648 (InSAR)-based kinematics, *The Cryosphere*, 18, 2335–2356, <https://doi.org/10.5194/tc-18-2335-2024>, 2024.

649 Berzescu, O., Ardelean, F., Urdea, P., Ioniță, A., and Onaca, A.: Thermal regime characteristics of alpine springs in the
650 marginal periglacial environment of the Southern Carpathians, *Sustainability*, in press, 2025.

651 Brencher, G., Handwerger, A.L., and Munroe, J.S.: InSAR-based characterization of rock glacier movement in the Uinta
652 Mountains, Utah, USA, *The Cryosphere*, 15, 4823–4844, <https://doi.org/10.5194/tc-15-4823-2021>, 2021.

653 Cicoira, A., Beutel, J., Faillettaz, J., and Vieli, A.: Water controls the seasonal rhythm of rock glacier flow, *Earth Planet. Sc.*
654 *Lett.*, 528, 115844, <https://doi.org/10.1016/j.epsl.2019.115844>, 2019.

655 Cicoira, A., Marcer, M., Gärtner-Roer, I., Bodin, X., Arenson, L. U., Vieli, A.: A general theory of rock glacier creep based
656 on in-situ and remote sensing observations, *Permafrost Periglac.*, 32, 139–153, <https://doi.org/10.1002/ppp.2090>, 2021.

657 Colucci, R.R., Forte, E., Žebre, M., Maset, E., Zanettini, C., and Guglielmin, M.: Is that a relict rock glacier?, *Geomorphology*,
658 330, 177–189, <https://doi.org/10.1016/j.geomorph.2019.02.002>, 2019.

659 Crosetto, M., Monserrat, O., Cuevas-González, M., Devanthery, N., and Crippa, B.: Persistent Scatterer Interferometry: A
660 review. *ISPRS J. Photogramm.*, 115, 78–89, <http://dx.doi.org/10.1016/j.isprsjprs.2015.10.011>, 2016.

661 Delaloye, R., and Lambiel, C.: Evidence of winter ascending air circulation throughout talus slopes and rock glaciers situated
662 in the lower belt of alpine discontinuous permafrost (Swiss Alps), *Nor. Geogr. Tidsskr.*, 59, 194–203,
663 <https://doi.org/10.1080/00291950510020673>, 2005.

664 Delaloye, R., Morard, S., Barboux, C., Abbet, D., Gruber, V., Riedo, M., and Gachet, S.: Rapidly moving rock glaciers in
665 Mattertal. In: *Graf, C.* (ed.) *Mattertal – ein Tal in Bewegung*. Publikation zur Jahrestagung der Schweizerischen
666 Geomorphologischen Gesellschaft 29. Juni – 1. Juli 2011, St. Niklaus. Birmensdorf, Eidg. Forschungsanstalt WSL. 21–30,
667 2013. Eriksen, H. Ø., Rouyet, L., Lauknes, T. R., Berthling, I., Isaksen, K., Hindberg, H., Larsen, Y., and Corner, G. D.: Recent
668 Acceleration of a Rock Glacier Complex, Ádjet, Norway, Documented by 62 Years of Remote Sensing Observations,
669 *Geophys. Res. Lett.*, 45, 8314–8323, <https://doi.org/10.1029/2018GL077605>, 2018.

670 European Environment Agency (EEA): EGMS Algorithm Theoretical Basis Document (ATBD), Copernicus Land Monitoring
671 Service, (<https://land.copernicus.eu/en/technical-library/egms-algorithm-theoretical-basis-document/@@download/file>),
672 accessed 18 April 2025.

673 Farbroth, H., Etzelmüller, B., Guðmundsson, Á., Humlum, O., Kellerer-Pirklbauer, A., Eiken, T., and Wangensteen, B.: Rock
674 glaciers and permafrost in Tröllaskagi, Northern Iceland, *Z. Geomorphol.*, 51, 1–16, <https://doi.org/10.1127/0372-8854/2007/0051s2-0001>, 2007.

675
676 Haeberli, W.: Die Basis-Temperatur der winterlichen Schneedecke als möglicher Indikator für die Verbreitung von Permafrost
677 in den Alpen, *Zeitschrift für Gletscherkunde und Glazialgeologie*, 9, 221–227, 1973.

678 Haeberli, W., Hallet, B., Arenson, L., Elconin, R., Humlum, O., Kääb, A., Kaufmann, V., Ladanyi, B., Matsuoka, N.,
679 Springman, S., and Mühll, D.V.: Permafrost creep and rock glacier dynamics, *Permafrost Periglac.*, 17, 189–214,
680 <https://doi.org/10.1002/ppp.561>, 2006.

681 Hartl, L., Zieher, T., Bremer, M., Stocker-Waldhuber, M., Zahs, V., Höfle, B., Klug, C., and Cicoira, A.: Multi-sensor
682 monitoring and data integration reveal cyclical destabilization of the Äußeres Hochebenkar rock glacier, *Earth Surf. Dynam.*,
683 11, 117–147, <https://doi.org/10.5194/esurf-11-117-2023>, 2023.

684 Hauck, C., Böttcher, M., and Maurer, H.: A new model for estimating subsurface ice content based on combined electrical and
685 seismic data sets, *The Cryosphere*, 5, 453–468, <https://doi.org/10.5194/tc-5-453-2011>, 2011.

686 Hausmann, H., Krainer, K., Brückl, E., and Mostler, W.: Internal structure and ice content of Reichenkar rock glacier (Stubai
687 Alps, Austria) assessed by geophysical investigations, *Permafrost Periglac.*, 18, 351–367, <https://doi.org/10.1002/ppp.601>,
688 2007.

689 Hawker, L., Uhe, P., Paulo, L., Sosa, J., Savage, J., Sampson, C., and Neal, J.: A 30 m global map of elevation with forests
690 and buildings removed. *Environ. Res. Lett.*, 17(2), 2022.

691 Herring, T., Lewkowicz, A. G., Hauck, C., Hilbich, C., Mollaret, C., Oldenborger, G. A., Uhlemann, S., Farzamian, M.,
692 Calmels, F., and Scandroglio, R.: Best practices for using electrical resistivity tomography to investigate permafrost,
693 *Permafrost Periglac.*, 34, 494–512, <https://doi.org/10.1002/ppp.2207>, 2023.

694 Hoelzle, M.: Permafrost occurrence from BTS measurements and climatic parameters in the eastern Swiss Alps, *Permafrost*
695 *Periglac.*, 3, 143–147, <https://doi.org/10.1002/ppp.3430030212>, 1992.

696 Hoelzle, M., Wegmann, M., and Krummenacher, B.: Miniature temperature dataloggers for mapping and monitoring of
697 permafrost in high mountain areas: First experience from the Swiss Alps, *Permafrost Periglac.*, 10, 113–124,
698 10.1002/(SICI)1099-1530(199904/06)10:23.0.CO;2-A, 1999.

699 Hu, Y., Arenson, L. U., Barboux, C., Bodin, X., Cicoira, A., Delaloye, R., Gärtner-Roer, I., Kääb, A., Kellerer-Pirklbauer, A.,
700 Lambiel, C., Liu, L., Pellet, C., Rouyet, L., Schoeneich, P., Seier, G., and Strozzi, T.: Rock glacier velocity: An Essential
701 Climate Variable Quantity for Permafrost, *Rev. Geophys.*, 63(1), e2024RG000847, <https://doi.org/10.1029/2024RG000847>,
702 2025.

703 Ishikawa, M., Fukui, K., Aoyama, M., Ikeda, A., Sawada, Y., and Matsuoka, N.: Mountain permafrost in Japan: Distribution,
704 landforms and thermal regimes, *Z. Geomorphol. Supp.*, 130, 99–116, 2003.

705 Kääb, A., Frauenfelder, R. and Roer, I.: On the response of rockglacier creep to surface temperature increase, *Glob. Planet.*
706 *Change*, 56, 172–187, <https://doi.org/10.1016/j.gloplacha.2006.07.005>, 2007.

707 Kääb, A., Strozzi, T., Bolch, T., Caduff, R., Trefall, H., Stoffel, M., and Kokarev, A.: Inventory and changes of rock glacier
708 creep speeds in Ile Alatau and Kungöy Ala-Too, northern Tien Shan, since the 1950s, *The Cryosphere*, 15, 927–949,
709 <https://doi.org/10.5194/tc-15-927-2021>, 2021.

710 Kääb, A. and Røste, A.: Rock glaciers across the United States predominantly accelerate coincident with rise in air
711 temperatures, *Nat. Commun.*, 15, 7581, <https://doi.org/10.1038/s41467-024-52093-z>, 2024.

712 Kellerer-Pirklbauer, A., Wangenstein, B., Farbroth, H., and Etzelmüller, B.: Relative surface age-dating of rock glacier systems
 713 near Hólar in Hjaltdalur, northern Iceland, *J. Quaternary Sci.*, 23, 137–151, <https://doi.org/10.1002/jqs.1117>, 2008.

714 Kellerer-Pirklbauer, A., Lieb, G.K., and Kleinfierchner, H.: A new rock glacier inventory of the eastern European Alps,
 715 *Austrian J. Earth Sci.*, 105, 78–93, 2012.

716 Kellerer-Pirklbauer, A.: Long-term monitoring of sporadic permafrost at the eastern margin of the European Alps
 717 (Hochreichart, Seckauer Tauern range, Austria), *Permafrost Periglac.*, 30, 260–277, <https://doi.org/10.1002/ppp.2021>, 2019.

718 Kellerer-Pirklbauer, A., Lieb, G.K., Kaufmann, V.: Rock Glaciers in the Austrian Alps: A General Overview with a Special
 719 Focus on Dösen Rock Glacier, Hohe Tauern Range. In: Embleton-Hamann, C. (eds) *Landscapes and Landforms of Austria*.
 720 *World Geomorphological Landscapes*. Springer, Cham, pp. 393–406, https://doi.org/10.1007/978-3-030-92815-5_27,
 721 2022.

722 Kellerer-Pirklbauer, A., Bodin, X., Delaloye, R., Lambiel, C., Gärtner-Roer, I., Bonnefoy-Demongeot, M., Carturan, L.,
 723 Damm, B., Eulenstein, J., Fischer, A., Hartl, L., Ikeda, A., Kaufmann, V., Krainer, K., Matsuoka, N., Di Cella, U.M., Noetzli,
 724 J., Seppi, R., Scapozza, C., Schoeneich, P., Stocker-Waldhuber, M., Thibert, E., and Zumiani, M.: Acceleration and interannual
 725 variability of creep rates in mountain permafrost landforms (rock glacier velocities) in the European Alps in 1995–2022,
 726 *Environ. Res. Lett.*, 19, 034022, <https://doi.org/10.1088/1748-9326/ad25a4>, 2024.

727 Kenner, R., Pruessner, L., Beutel, J., Limpach, P., and Phillips, M.: How rock glacier hydrology, deformation velocities and
 728 ground temperatures interact: Examples from the Swiss Alps, *Permafrost Periglac.*, 31, 3–14,
 729 <https://doi.org/10.1002/ppp.2023>, 2020.

730 LAKE II MNT: Agentia Nationala de Cadastru si Publicitate Imobiliara: Land Administration Knowledge Improvement,
 731 available online: geoportal.ancpi.ro last acces: 01.09.2024, 2024.

732 Lambiel, C., Strozzi, T., Paillex, N., Vivero, S., and Jones, N.: Inventory and kinematics of active and transitional rock glaciers
 733 in the Southern Alps of New Zealand from Sentinel-1 InSAR, *Arctic Antarct. Alp. Res.*, 55, 2183999,
 734 <https://doi.org/10.1080/15230430.2023.2183999>, 2023.

735 Lilleøren, K.S., Etzelmüller, B., Rouyet, L., Eiken, T., Slinde, G., and Hilbich, C.: Transitional rock glaciers at sea level in
 736 northern Norway, *Earth Surf. Dynam.*, 10, 975–996, <https://doi.org/10.5194/esurf-10-975-2022>, 2022.

737 Liu, L., Millar, C.I., Westfall, R.D., and Zebker, H.A.: Surface motion of active rock glaciers in the Sierra Nevada, California,
 738 USA: Inventory and a case study using InSAR, *The Cryosphere*, 7, 1109–1119, <https://doi.org/10.5194/tc-7-1109-2013>, 2013.

739 Marcer, M., Cicoira, A., Cusicanqui, D., Bodin, X., Echelard, T., Obregon, R., and Schoeneich, P.: Rock glaciers throughout
 740 the French Alps accelerated and destabilised since 1990 as air temperatures increased, *Commun. Earth Environ.*, 2,
 741 <https://doi.org/10.1038/s43247-021-00150-6>, 2021.

742 Mollaret, C., Wagner, F.M., Hilbich, C., Scapozza, C., and Hauck, C.: Petrophysical Joint Inversion Applied to Alpine
 743 Permafrost Field Sites to Image Subsurface Ice, Water, Air, and Rock Contents, *Front. Earth Sci.*, 8, 85,
 744 <https://doi.org/10.3389/feart.2020.00085>, 2020.

744 Necsoiu, M., Onaca, A., Wigginton, S., and Urdea, P.: Rock glacier dynamics in Southern Carpathian Mountains from high-
 745 resolution optical and multi-temporal SAR satellite imagery, *Remote Sens. Environ.*, 177, 21–36,
 746 <https://doi.org/10.1016/j.rse.2016.02.025>, 2016.

747 Oliva, M., Fernandes, M., Palacios, D., Fernández-Fernández, J.M., Schimmelpfennig, I., Antoniades, D., Aumaître, G.,
 748 Bourlès, D., and Keddadouche, K.: Rapid deglaciation during the Bølling-Allerød Interstadial in the Central Pyrenees and
 749 associated glacial and periglacial landforms, *Geomorphology*, 385, 107735, <https://doi.org/10.1016/j.geomorph.2021.107735>,
 750 2021.

751 Onaca, A.L., Urdea, P., and Ardelean, A.C.: Internal structure and permafrost characteristics of the rock glaciers of Southern
 752 Carpathians (Romania) assessed by geoelectrical soundings and thermal monitoring, *Geogr. Ann. A.*, 95, 249–266,
 753 <https://doi.org/10.1111/geoa.12014>, 2013.

754 Onaca, A., Ardelean, A.C., Urdea, P., Ardelean, F., and Sirbu, F.: Detection of mountain permafrost by combining
 755 conventional geophysical methods and thermal monitoring in the Retezat Mountains, Romania, *Cold Reg. Sci. Technol.*, 119,
 756 111–123, <https://doi.org/10.1016/j.coldregions.2015.08.001>, 2015.

757 Onaca, A., Urdea, P., Ardelean, A.C., Șerban, R., and Ardelean, F.: Present-day periglacial processes in the alpine zone, in:
 758 *Landform Dynamics and Evolution in Romania*, edited by: Rădoane, M., Vespremeanu-Stroe, A., Springer Geography, 147-
 759 176, 2017a.

760 Onaca, A., Ardelean, F., Urdea, P., and Magori, B.: Southern Carpathian rock glaciers: Inventory, distribution and
 761 environmental controlling factors, *Geomorphology*, 293, 391–404, <http://dx.doi.org/10.1016/j.geomorph.2016.03.032>, 2017b.

762 Onaca, A., Ardelean, F., Ardelean, A., Magori, B., Sirbu, F., Voiculescu, M., and Gachev, E.: Assessment of permafrost
 763 conditions in the highest mountains of the Balkan Peninsula, *Catena*, 185, 104288,
 764 <https://doi.org/10.1016/j.catena.2019.104288>, 2020.

765 Noetzli, J., Isaksen, K., Christiansen, H., Delaloye, R., Etzelmüller, B., Farinotti, D., Galleman, T., Guglielmin, M., Hauck,
 766 C., Hilbich, C., Hoelzle, M., Lambiel, C., Magnin, F., Oliva, M., Paro, L., Pogliotti, P., Riedl, C., Schoeneich, P., Valt, M.,
 767 Vieli, M., and Philips, M.: Enhanced warming of European mountain permafrost in the early 21st century, *Nat. Commun.*, 15,
 768 10508, <https://doi.org/10.1038/s41467-024-54831-9>, 2024.

769 Pavelescu, L.: Studiu geologic și petrografic al regiunii centrale și de sud-est a Munților Retezat [Geological and petrographic
 770 study of the central and south-eastern region of the Retezat Mountains], *AIGR*, XXV, 119-210, 1953.

771 Pandey, P., Nawaz Ali, S., Subhasmita Das, S., and Ataullah Raza Khan, M.: Rock glaciers of the semi-arid northwestern
 772 Himalayas: distribution, characteristics, and hydrological significance, *Catena*, 238, 107845,
 773 <https://doi.org/10.1016/j.catena.2024.107845>, 2024.

774 Pellet, C., Bodin, X., Cusicanqui, D., Delaloye, R., Kääb, A., Kaufmann, V., Thibert, E., Vivero, S., and Kellerer-Pirklbauer,
 775 A.: Rock glacier velocity. In: *State of the Climate in 2023*, *Bull. Am. Meteorol. Soc.*, 105, 44–46,
 776 <https://doi.org/10.1175/2024BAMSStateoftheClimate.1>, 2024.

777 Poncoş, V., Stanciu, I., Teleagă, D., Maţenco, L., Bozsó, I., Szakács, A., Birtas, D., Toma, Ş.A., Stănică, A., and Rădulescu,
778 V.: An Integrated Platform for Ground-Motion Mapping, Local to Regional Scale; Examples from SE Europe, *Remote Sens-*
779 *Basel.*, 14, 1046, <https://doi.org/10.3390/rs14041046>, 2022.

780 Popescu, R., Vespremeanu-Stroe, A., Onaca, A., and Cruceru, N.: Permafrost research in the granitic massifs of Southern
781 Carpathians (Parâng Mountains), *Z. für Geomorphol.*, 59(1), 1-20, doi.org/10.1127/0372-8854/2014/0145, 2015.

782 Popescu, R., Onaca, A., Urdea, P., and Vespremeanu-Stroe, A.: Spatial Distribution and Main Characteristics of Alpine
783 Permafrost from Southern Carpathians, Romania, In Rădoane, M., Vespremeanu-Stroe, A. (Eds.), *Landform dynamics and*
784 *evolution in Romania*, Springer, 117-146, DOI: 10.1007/978-3-319-32589-7_6, 2017.

785 Popescu, R., Filhol, S., Etzelmüller, B., Vasile, M., Pleşoianu, A., Virghileanu, M., Onaca, A., Şandric, I., Săvulescu, I.,
786 Cruceru, N., Vespremeanu-Stroe, A., Westermann, S., Sîrbu, F., Mihai, B., Nedelea, A., and Gascoin, S.: Permafrost
787 Distribution in the Southern Carpathians, Romania, Derived From Machine Learning Modeling, *Permafrost Periglac.*, 35, 243–
788 261, <https://doi.org/10.1002/ppp.2232>, 2024.

789 Rangecroft, S., Harrison, S., and Anderson, K.: Rock glaciers as water stores in the Bolivian Andes: An assessment of their
790 hydrological importance, *Arct. Antarct. Alp. Res.*, 47, 89–98, <https://doi.org/10.1657/AAAR0014-029>, 2015.

791 RGIK: Guidelines for inventorying rock glaciers: baseline and practical concepts (version 1.0). IPA Action Group Rock glacier
792 inventories and kinematics, 25, DOI:10.51363/unifr.srr.2023.002, 2023a.

793 RGIK: InSAR-based kinematic attribute in rock glacier inventories. Practical InSAR Guidelines (version 4.0., 31.05.2023),
794 IPA Action Group Rock Glacier Inventories and Kinematics (RGIK), 33 pp, www.rgik.org, 2023b.

795 Roer, I., Haeberli, W., Avian, M., Kaufmann, V., Delaloye, R., Lambiel, C., and Kääb, A.: Observations and considerations
796 on destabilizing active rock glaciers in the European Alps, in: *Proc. Ninth Int. Conf. on Permafrost*, Fairbanks, Alaska, 29
797 June–3 July 2008, Kane, D. L. and Hinkel, K. M. (Eds.), Institute of Northern Engineering, University of Alaska, pp. 1505–
798 1510, 2008.

799 Rouyet, L., Lilleoren, K.S., Boehme, M., Vick, L.M., Delaloye, R., Etzelmüller, B., Lauknes, T.R., Larsen, Y., and Blikra,
800 L.H.: Regional Morpho-Kinematic Inventory of Slope Movements in Northern Norway, *Front. Earth Sci.* 9, 681088,
801 <https://doi.org/10.3389/feart.2021.681088>, 2021.

802 Rucci, A., Ferretti, A., Monti Guarnieri, A., and Rocca, F.: Sentinel 1 SAR interferometry applications: The outlook for sub
803 millimeter measurements, *Remote Sens. Environ.*, 120, 156–163, <https://doi.org/10.1016/j.rse.2011.09.030>, 2012.

804 Rücker, C., Günther, T., and Wagner, F.M.: pyGIMLi: An open-source library for modelling and inversion in geophysics,
805 *Comput. Geosci.*, 109, 106–123, <https://doi.org/10.1016/j.cageo.2017.07.011>, 2017.

806 Ruszkiczay-Rüdiger, Z., Kern, Z., Urdea, P., Madarász, B., Braucher, R., and ASTER Team: Limited glacial erosion during
807 the last glaciation in mid-latitude cirques (Retezat Mts, Southern Carpathians, Romania), *Geomorphology*, 384, 107719,
808 <https://doi.org/10.1016/j.geomorph.2021.107719>, 2021.

809 Sandmeier, K.-J.: REFLEXW Version 9.1.3. Windows™ XP/7/8/10-program for the processing of seismic, acoustic or
810 electromagnetic reflection, refraction and transmission data, 2020.

811 Santos-González, J., González-Gutiérrez, R.B., Redondo-Vega, J.M., Gómez-Villar, A., Jomelli, V., Fernández-Fernández,
812 J.M., Andrés, N., García-Ruiz, J.M., Peña-Pérez, S.A., Melón-Nava, A., Oliva, M., Álvarez-Martínez, J., Charton, J., ASTER
813 Team, and Palacios, D.: The origin and collapse of rock glaciers during the Bølling-Allerød interstadial: A new study case
814 from the Cantabrian Mountains (Spain), *Geomorphology*, 401, 108112, <https://doi.org/10.1016/j.geomorph.2022.108112>,
815 2022.

816 Sattler, K., Anderson, B., Mackintosh, A., Norton, K., and de Róiste, M.: Estimating permafrost distribution in the maritime
817 Southern Alps, New Zealand, based on climatic conditions at rock glacier sites, *Front. Earth Sci.*, 4, 4,
818 <https://doi.org/10.3389/feart.2016.00004>, 2016.

819 Schoeneich, P.: Guide lines for monitoring GST – Ground surface temperature, PERMANET project, Version 3 – 2.2.2011,
820 <https://www.permanet-alpinespace.eu/archive/pdf/GST.pdf>, 2011, accessed 20 April 2025.

821 Scotti, R., Brardinoni, F., Alberti, S., Frattini, P., and Crosta, G.B.: A regional inventory of rock glaciers and protalus ramparts
822 in the central Italian Alps, *Geomorphology*, 186, 136–149, <https://doi.org/10.1016/j.geomorph.2012.12.028>, 2013.

823 Serrano, E., de Sanjosé, J.J., and González-Trueba, J.J.: Rock glacier dynamics in marginal periglacial environments, *Earth*
824 *Surf. Proc. Land.*, 35, 1302–1314, <https://doi.org/10.1002/esp.1972>, 2010.

825 Steinemann, O., Reitner, J.M., Ivy-Ochs, S., Christl, M., and Synal, H.-A.: Tracking rockglacier evolution in the Eastern Alps
826 from the Lateglacial to the early Holocene, *Quaternary Sci. Rev.*, 241, 106424,
827 <https://doi.org/10.1016/j.quascirev.2020.106424>, 2020.

828 Stiegler, C., Rode, M., Sass, O., and Otto, J.C.: An Undercooled Scree Slope Detected by Geophysical Investigations in
829 Sporadic Permafrost below 1000 M ASL, Central Austria, *Permafrost Periglac.*, 25, 194–207,
830 <https://doi.org/10.1002/ppp.1813>, 2014.

831 Strozzi, T., Caduff, R., Jones, N., Barboux, C., Delaloye, R., Bodin, X., Kääb, A., Mätzler, E., and Schrott, L.: Monitoring
832 rock glacier kinematics with satellite synthetic aperture radar, *Remote Sens.-Basel.*, 12, 559,
833 <https://doi.org/10.3390/rs12030559>, 2020.

834 Timur, A.: Velocity of compressional waves in porous media at permafrost temperatures, *Geophysics*, 33, 584–595,
835 <https://doi.org/10.1190/1.1439954>, 1968.

836 Urdea, P.: Permafrost and periglacial forms in the Romanian Carpathians, in: 6th International Conference on Permafrost,
837 South China University of Technology, Beijing, China, 631–637, 1993.

838 Urdea, P.: Munții Retezat, Studiu geomorfologic [Retezat Mountains. A geomorphological study], Academiei, București, 272
839 pp, ISBN 973-27-0767-4, 2000.

840 Vespremeanu-Stroe, A., Urdea, P., Popescu, R., and Vasile, M.: Rock Glacier Activity in the Retezat Mountains, Southern
841 Carpathians, Romania, *Permafrost Periglac.*, 23, 127–137, <https://doi.org/10.1002/ppp.1736>, 2012.

842 Vonder Mühll, D., Hauck, C., and Gubler, H.: Mapping of mountain permafrost using geophysical methods, *Prog. Phys. Geog.*,
843 26, 643–660, <https://doi.org/10.1191/0309133302pp356ra>, 2002.

844 Wagner, F.M., Mollaret, C., Günther, T., Kemna, A., and Hauck, C.: Quantitative imaging of water, ice and air in permafrost
845 systems through petrophysical joint inversion of seismic refraction and electrical resistivity data, *Geophys. J. Int.*, 219, 1866–
846 1875, <https://doi.org/10.1093/gji/ggz402>, 2019.

847 Wagner, T., Seelig, S., Helfricht, K., Fischer, A., Avian, M., Krainer, K., and Winkler, G.: Assessment of liquid and solid
848 water storage in rock glaciers versus glacier ice in the Austrian Alps, *Sci. Total Environ.*, 800, 149593,
849 <https://doi.org/10.1016/j.scitotenv.2021.149593>, 2021.

850 Wicky, J. and Hauck, C.: Numerical modelling of convective heat transport by air flow in permafrost talus slopes, *The*
851 *Cryosphere*, 11, 1311–1325, <https://doi.org/10.5194/tc-11-1311-2017>, 2017.

852 Wirz, V., Gruber, S., Purves, R.S., Beutel, J., Gärtner-Roer, I., Gubler, S., and Vieli, A.: Short-term velocity variations at three
853 rock glaciers and their relationship with meteorological conditions, *Earth Surf. Dynam.*, 4, 103–123,
854 <https://doi.org/10.5194/esurf-4-103-2016>, 2016.

855 Yu, J., Meng, X., Yan, B., Xu, B., Fan, Q., and Xie, Y.: Global Navigation Satellite System-based positioning technology for
856 structural health monitoring: a review, *Struct. Control. Hlth.*, 27, 2467, <https://doi.org/10.1002/stc.2467>, 2020.

857